A Power Converter for Photovoltaic Applications

Björn Lindgren

Department of Electric Power Engineering
CHALMERS UNIVERSITY OF TECHNOLOGY
Göteborg, Sweden 2000

A Power Converter for Photovoltaic Applications

Björn Lindgren

Technical Report No. 335L

Submitted to the School of Electrical and Computer Engineering
Chalmers University of Technology
In partial fulfilment for a Licentiate of Engineering Degree

Department of Electric Power Engineering
Göteborg, Sweden
February, 2000

CHALMERS UNIVERSITY OF TECHNOLOGY
Department of Electric Power Engineering
SE-412 96 Göteborg
Chalmers Bibliotek, Reproservice
Göteborg, 2000

Abstract

The thesis describes some important considerations when using photovoltaics in producing energy to the main grid. The function of photovoltaic (PV) cells is briefly described, and the interaction between cells as miss-match and the hot-spot effect are explained in case PV-cells are connected in series. Simulations of how shading affects the overall performance are presented. The result shows a 48 % loss of energy when only 4.2 % of the area is shaded. Decentralised system configurations, such as string inverters and PV-module oriented inverters are described as a solution to PV installations in shaded areas. Different possible converter topologies are compared with respect to energy efficiency and cost. Based on an analysis an optimal configuration has been made for a demonstration photovoltaic power plant. Results of a designed 110 W low voltage inverter are presented showing a high energy-efficiency of 94 % and a low distortion on the grid with a THD_i of 8.8 % for all frequencies.

Keywords: Inverters, Photovoltaic power systems, Solar power generation, Fault tolerance, Bang-bang control, Current control, MOSFET circuits, Shading effects, Miss-match.

Preface

The work involved in this study has been carried out at the Department of Electric Power Engineering, Chalmers University of Technology. The project is part of a larger project called PROPHECY, which focuses on solar produced electricity and the storage of electric energy in batteries and hydrogen. Activity centre is a demonstration photovoltaic power plant a few kilometres north of the city of Göteborg called Sankt Jörgen.

I would like to thank my supervisor Docent Ola Carlson for his support during this work. My sincere thanks to Professor Jaap Daalder as my examiner.

The Research Foundation at Göteborg Energi AB is gratefully acknowledged for its financial support. Thanks are also due to the members of the Reference Group, Kjell Jonasson (Göteborg Energi), Ola Gröndalen (Sydkraft) and Per Johander (IVF).

Finally, I would like to thank my colleagues of the department for their good companionship.

List of Included Papers

Paper A

B. Lindgren, P. Carlsson and L. Cider
"Yield Losses due to Shading in a Building-integrated PV Installation; Evaluation, Simulation and Suggestions for Improvements", Published at the 2nd World Conference and Exhibition on Photovoltaic Solar Energy Conversion, Vienna 1998.

Paper B

Björn Lindgren
"Topology for Decentralised Solar Energy Inverters with a Low Voltage AC-Bus", Published at the 8th European Conference on Power Electronics an Applications (EPE'99), Lausanne, Switzerland, 7-9 September 1999.

Paper C

Björn Lindgren
”A 110 W Inverter for Photovoltaic Applications”, submitted to IEEE transactions on Energy Conversion, Energy Development and Power Generation Committee.

Table of Contents

1. Introduction

Most people, who are environmentally aware and are familiar with energy technology, agree that energy from the sun has extraordinary advantages when compared with other sources. Basically, solar energy has zero emission and if manufacturing and recycling can be properly performed an extremely clean and abundant supply of energy will be attained for centuries.

Besides hydrogen power and wind power, which also originate from the sun, the utilising of solar energy can be divided into two separate branches. These two branches are thermal solar energy and photovoltaic solar energy. The former is the most mature technology and in many cases the least expensive but has a disadvantage: the energy output is heat and the efficiency is only high if heat is required. Often heat is not needed during the sunny season.

This work deals with energy production using photovoltaics. The advantage of this technique compared with thermal heat is that the solar energy is converted to a very versatile form, electricity. This is an energy form that can easily be used locally, transported or even stored, although the storage methods can be refined and developed further. Thermal heat can also be converted into electricity, but the high efficiency is drastically reduced in a heat-to-work conversion which leads to an efficiency of the same order as for photovoltaics.

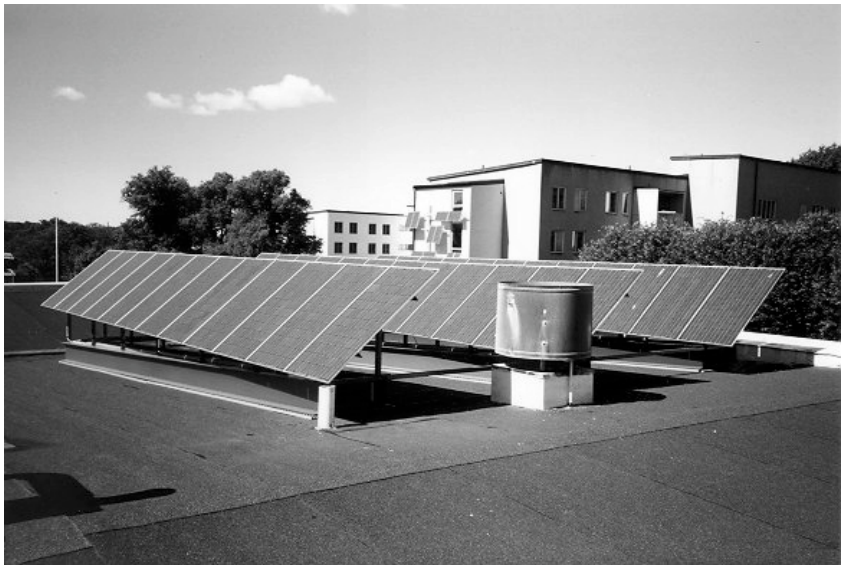

Figure 1. The Sankt Jörgen photovoltaic power plant.

In 1995, a demonstration photovoltaic power plant was inaugurated at Sankt Jörgen, Göteborg, Sweden, Figure 1. It was funded by the Research Foundation of Göteborg Energi AB and was realised in co-operation with Göteborg University and Chalmers University of Technology. The plant is a base for building up knowledge in the photovoltaic area. At Sankt Jörgen, 48 photovoltaic modules each consisting of 72 cells and having an area of 0.9 m^2, are connected through an inverter to the public grid. Twelve PV-modules are connected to a DC/DC-converter feeding a 48 V battery system. All together the installed peak power is 6.6 kW.

In 1997, an evaluation of the power plant was performed. The result was discouraging due to shading and poor design. This is not a unique situation, see [1][2][3][4]. **Paper A** describes a method for simulating the expected energy production of a solar power plant and compares the expected production with the actual energy yield. It also discusses some of the mistakes made at

Sankt Jörgen and suggests a number of measures that would improve the performance of the power plant.

One suggestion to improve the performance is to decentralise the power conversion [5][6][7], thus making the PV-plant more shade-tolerant. **Paper B** compares a number of possible configurations of PV-modules and inverter topologies and suggests a PV-module oriented inverter that would improve the energy yield of the power plant.

A PV-module inverter has been designed and constructed. In **Paper C** some results of the design are presented. The current controller has been implemented in an inexpensive 8-bit micro controller, which uses a hysteresis technique also known as bang-bang control. The emphasis is on high energy-efficiency and high power quality.

2. Photovoltaics

The photovoltaic effect is described in Encyclopaedia Britannica as "a process in which two dissimilar materials in close contact act as an electric cell when struck by light or other radiant energy".

2.1 History

In 1839, Edmund Becquerel, the French experimental physicist, discovered the photovoltaic effect while experimenting with an electrolytic cell made up of two metal electrodes placed in an electricity-conducting solution. The generation of electric power increased when exposed to light. During the 19th century, a few other notable events took place which dealt with the photovoltaic effect in different semiconductors.

In 1904, Albert Einstein, published a paper explaining the phenomenon for which he received the Nobel Prize in 1921.

By this time, the photovoltaic effect was not applicable to energy-generation due to the low efficiency (< 0.5 %), the need of rare and expensive materials and a lack of industrial production methods. It was in 1954 that Bell Laboratories reported on a working silicon photovoltaic cell with an efficiency of 4.5 % thus making the cells of interest for power generation. They were primarily intended for application in space, where it is expensive to supply electronics with energy for a long time. Only four years later, the first satellite with photovoltaics, the US Vaguard, was launched.

Since then, new records for the maximum efficiency of photovoltaics have constantly been set. For laboratory samples, the record is now above 30 %, for space applications the efficiency is well above 25 %, while the efficiency of commercial PV-cells ranges from 8 to 16 %. The price, however, is still too high to compete with conventional energy sources with the exception of remote applications. For example in light houses the PV can be the best choice from an economic point of view. Applications in electronic devices, such as calculators and clocks are also well known.

For the developing countries, the PV offers great potential to increase the standard of living in un-electrified rural places where the weather is fairly sunny. It is relatively easy to have a radio receiver and a refrigerator run on a lead-acid battery that is charged during the day by PV-cells. This solution is far less expensive when compared with installing power lines to every remote building.

2.2 Four Types of Photovoltaic Cells

The majority of photovoltaic cells are made from crystalline silicon, see Figure 2. Mostly mono crystalline material rejected by the electronic industry for reasons of impurity, is used. The cell can also be made from multi-crystalline material, where the step is skipped in which a mono crystal is slowly grown from a small seed to a large ingot. This makes these cells less expensive while the efficiency becomes somewhat lower, 10-13 % as compared with 12-16 % for commercial mono crystalline. Two disadvantages with these types are that they cannot easily be produced in larger sizes and they require enormous investments in clean-room factories. The energy payback time is also quite long due to the power consuming processes required for refining silicone.

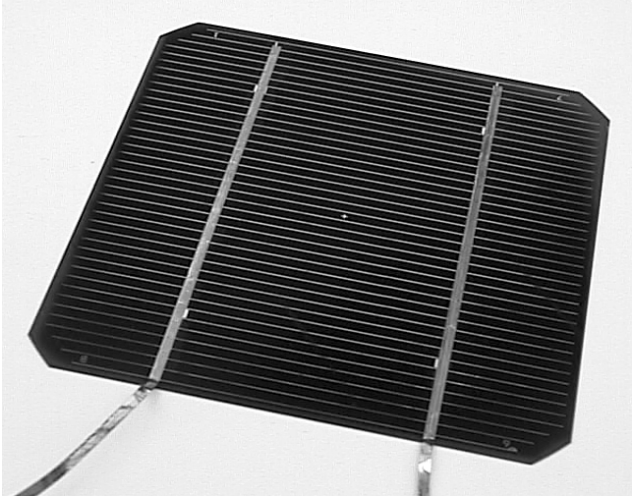

Figure 2. A mono crystalline photovoltaic cell of silicon.

In 1974, amorf silicon was used for the first time. This opened the way for a new type of PV-cells called thin-film photovoltaic cells. Actually, this family includes several different materials as amorf silicon (a-Si), CdTe, CIGS and GaAs. A common feature of these PV-cells is that the semiconductors are applied to a surface in very thin layers (a few μm). The advantages are that less semiconductor material is used, the expensive and energy-consuming process for making the mono crystalline ingots is skipped, and finally it is possible to make large PV-modules in a fully automated process. Pilkington is producing up to 6 m^2 PV-modules today.

The third type is the Dye Sensitised Solar Cell (DYSC), or Grätzel-cell as it is often referred to, after its inventor Michael Grätzel, Switzerland. Instead of two solid-state semiconductors, a dye solution and a solid state semiconductor (TiO_2) are employed. The advantage of this type is that the cells can be produced at a relatively low cost. No clean room is needed, which makes them attractive for developing countries. At low light irradiation, such as in indoor applications, these cells are more favourable as the efficiencies of the other types decrease and become of the same order as the dye-sensitised cell. The disadvantages of these cells, however, are their lower efficiency (5-8 %) and that they are not yet stable.

A type of PV-cell that at present has the highest value of efficiency (officially 32.6 %, February 2000) is called the multijunction cell (or tandem cell in case of two layers). It consists of two or more PV-cells stacked with different band gaps so each cell utilises different regions of the irradiated spectrum. These cells are not, to my knowledge, produced in any quantity but are laboratory samples in the order of some square centimetres.

2.3 The Photovoltaic Effect

A photovoltaic cell is a doped semiconductor so that an n-p-junction is obtained. This gives rise to an electric field inside the semiconductor. If a photon (a radiant energy quantum), hits an electron with high enough energy, it is torn off the atom and transported by the electric field to the other side of the junction, thus giving rise to a voltage across the junction. If an external load is connected between the n- and p-side, a DC-current will flow. The power from the photovoltaic cell depends on the light irradiation but also on the load and the temperature of the photovoltaic cell.

2.3.1 The Characteristic IV-curve

A photovoltaic cell is, as described above, a diode which is designed to promote the photovoltaic effect. In complete darkness, the voltage-current characteristic is described by the diode equation (Figure 3 and Equation (1)).

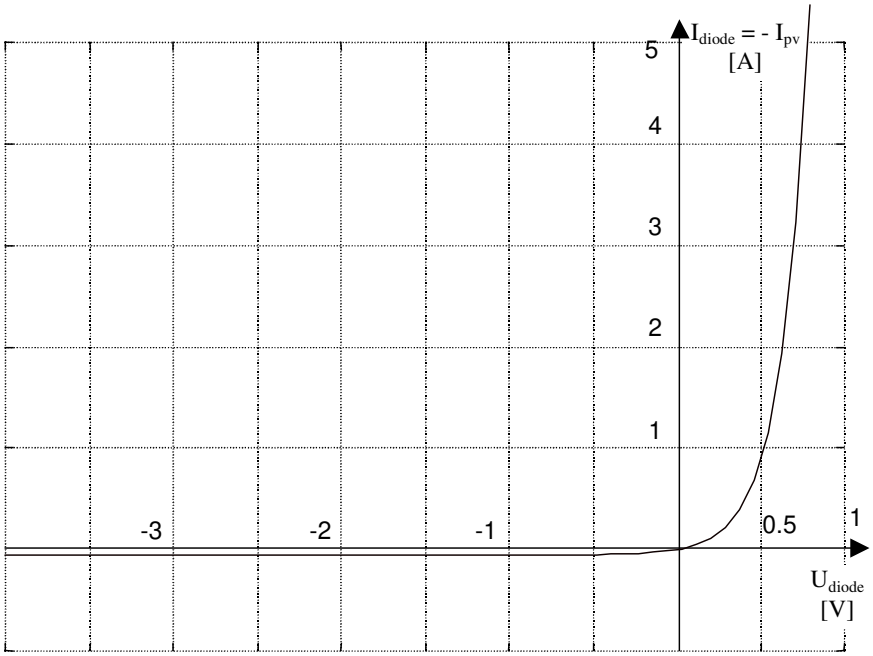

Figure 3. The typical iv-curve for a diode.

$$i_{diode} = C_{diode} \cdot T^{\frac{3}{n}} \cdot e^{-\frac{qU_g}{nkT}} \left(e^{\frac{qU_{diode}}{nkT}} - 1 \right) \qquad (1)$$

Here C_{diode} is a constant, T the temperature, n an ideality factor, q the electron charge, U_g the band gap of the semiconductor, k is the Boltzmann constant and U_{diode} the voltage across the diode.

When the PV-cell is illuminated, the iv-curve will move along the current axis (y-axis). In other words, it produces a current approximately proportional to the irradiated power. This is often modelled by electric schemes as in Figure 4 [8].

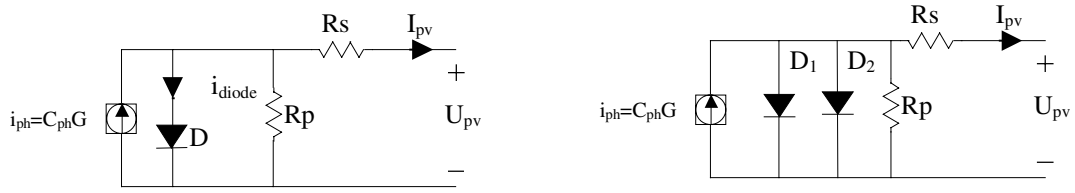

Figure 4. The one-diode and two-diode models of a photovoltaic cell.

The current source generates a current proportional to the irradiation G [W/m^2]. The diode behaviour is modelled with the parameters of the diode, D in Figure 4a. In cases where higher accuracy is needed, two diodes in parallel are often used, where one models the characteristics at high irradiation and the other models the low power range. This is known as the two-diode model

shown in Figure 4b. The parallel Resistor, R_p, models the leakage resistance of the semiconductor. R_s is the series resistance, i.e., the sum of the metalisation resistance and resistance in the semiconductor. To improve the model's temperature behaviour, the constant C_{ph} can be written as a polynomial of the temperature, see Equation (2).

$$C_{ph} = C_{ph0} + C_{ph1}(T_{25} - T) + C_{ph2}(T_{25} - T)^2 + \ldots \qquad (2)$$

In practice, the first two terms give quite a good approximation.

The iv-curves of a PV-cell (or the model above) are shown in Figure 5 at different levels of irradiation. Here the current axis is negative compared with the current axis in Figure 3.

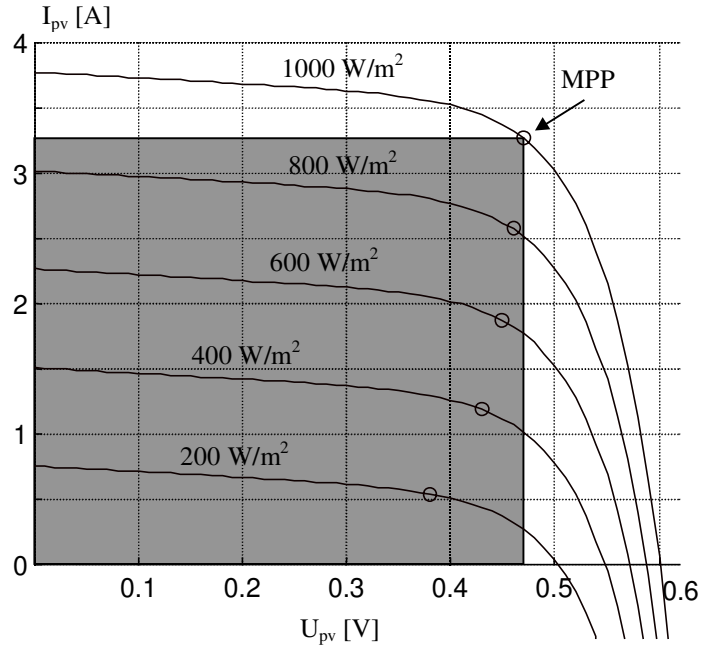

Figure 5. Typical iv-curves for PV-cells at different levels of irradiation.

At a an irradiation of 1000 W/m^2, corresponding approximately to a cloud-free, sunny day, the upper curve shows that the open-circuit voltage of the cell is about 0.6 V. As the load (current) of the cell increases, the voltage decreases and at short-circuit (voltage = 0) the current is approx. 3.7 A. At open circuit and at short-circuit, no power is produced (apart from small conducting losses in the latter case). At a point called the maximum power point (MPP), maximum power is gained from the PV-cell. To visualise where this point is located, a rectangle can be drawn from any point of the curve to its origin. For the point where this rectangle has the largest area maximum power is generated. Another, less obvious criterion is the point on the curve where its derivative is equal to the negative derivative of a straight line from the origin to the point.

At lower irradiation, the short-circuit current decreases approximately linearly with irradiation. The open circuit voltage does not decrease as much until at a very low irradiation. However, the open circuit voltage is much more affected by the temperature of the PV-cell. At a higher temperature, the open circuit voltage decreases. This is due to an increased probability that an excited electron will collide with an atom in the lattice, as a higher temperature means that the atoms in the lattice vibrate more and therefore have a larger virtual cross-section area. The electron, then, does not contribute to the driving current, but increases the vibration energy (temperature) of the lattice. The

phenomenon has quite a large impact and decreases the output power by approximately 15 % at a temperature increase from 25°C to 50°C.

2.3.2 Miss-match

As PV-cells have a relatively low voltage (0.5 V) they are almost always connected in series to obtain an appropriate voltage. If a higher current is needed, they can also be connected in parallel. For small equipment, such as clocks or calculators, 4-10 cells are often used. For more power demanding equipment, such as light-houses, the number of cells are matched to the battery storage used, normally lead-acid cells of 12-14 V, which makes a series connection of 32-36 PV-cells suitable. For larger PV-installations, there are no current standards for how many cells should be mounted on a module. The PV-modules at the 6.6 kW S:t Jörgen PV-plant have 72 cells in series per module.

What happens when PV-cells are connected in series? Assume N cells are connected in series to a load as shown in Figure 6.

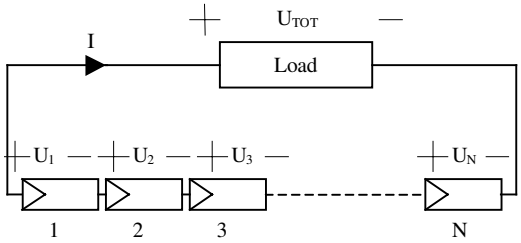

Figure 6. Series connected PV-cells and load.

Obviously, they will carry the same current (first law of Kirchoff) and the resulting voltage, U_{TOT}, will be the sum of the voltages of all the individual cells (second law of Kirchoff). If all cells have the same characteristics and are equally illuminated (i.e., identical iv-cures), they will behave as a single cell, but with a voltage N times higher and, therefore, N times the power of one cell. In reality, PV-cells cannot be produced identically and even if they could, they would not have identical temperatures, or worse, not always be illuminated equally in an installation. As they have to carry the same current, this means that they *all* cannot work at their MPP. Energy is lost because some cells in the series 'could have' produced more. This is known as miss-match, and manufactures are aware of this phenomenon. They normally sort their cells, to assemble cells having as close characteristics as is possible on the same module. But, when the modules are shipped to a new installation, modules can possibly be connected in series with quite dissimilar characteristics.

2.3.3 Shading

An extreme case of miss-match is a phenomenon called the hot spot effect. It can seriously endanger the function of the affected PV-cells. Assume one cell in Figure 6 is 75 % covered by a large leaf. Now we have a pronounced miss-match. The short-circuit current of the shaded cell is decreased by 75 % and the potential energy from the PV-series is drastically decreased. Exactly what happens depends on how many cells there are in the series and on the loading device. In the worst case, the shaded cell is forced into a reverse voltage and starts to dissipate power instead of producing. Hence, it is heated up and at temperatures above approx. 130°C its function starts to degenerate irretrievably.

To understand the hot-spot phenomenon, the second quadrant of the iv-curve and the reverse voltage break through, or the avalanche effect of a diode [9], must be considered. In Figure 7, the iv-curve for quadrants one and two is shown.

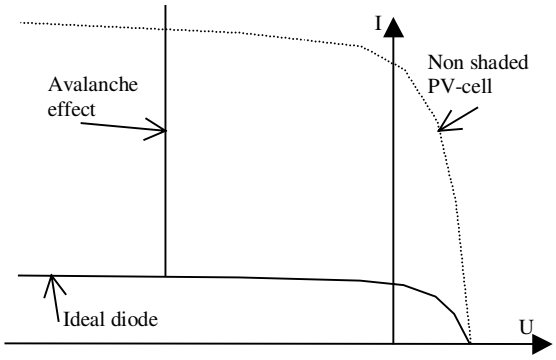

Figure 7. IV-curve for reversed voltage quadrant.

An ideal diode can withstand any reverse voltage and in the case of an ideal PV-cell it will work as a constant current load if reverse voltage is applied. In a series of PV-cells this means that the least illuminated cell will limit the current from the whole series. In reality, there is a point of break-through in the pn-junction when the externally applied electric field will overcome the intrinsic electric field, known as the avalanche effect. For a silicon PV-cell, this will happen at 14-30 V ($U_{avalanche}$). Subsequently, the maximum current through a series of PV-cells is no longer limited by the shaded cell, but the cell will dissipate power at the avalanche voltage times the current.

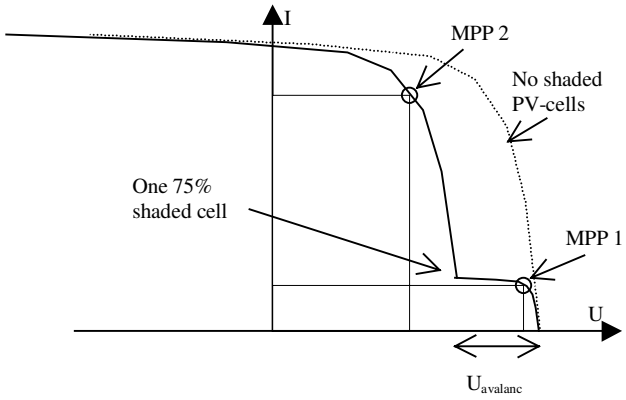

Figure 8. A series of PV-cells with one shaded cell.

Figure 8 shows the iv-curve of a series of PV-cells, where one cell is in 75 % shade . It can be noted that the curve now has two local maximum power points; MPP1 and MPP2. The one that is the over-all MPP, depends on how many cells there are in the series and on the $U_{avalanche}$.

In MPP 1, the shaded cell is not reversed, but produces energy at its MPP, while all the non-shaded cells just produce approx. 25 % of their potential energy production. In MPP 2, the shaded cell has a reversed voltage and consumes energy. The rest of the cells produce more energy than in MPP 1 (although not at their MPP).

To avoid the destruction of PV-cells due to this hot-spot effect, manufacturers connect by-pass diodes, for instance for a group of 8 cells, see Figure 9. With this arrangement a substring with a shaded cell will be short-circuited by the by-pass diode and the non-shaded substrings can work at their MPP, but the energy from the by-passed substring is lost. It is important to underline that this

is normally only a method for the protection of the PV-cells. If by-pass diodes are used to make the PV-module more shade-tolerant, they should be connected to significantly fewer PV-cells.

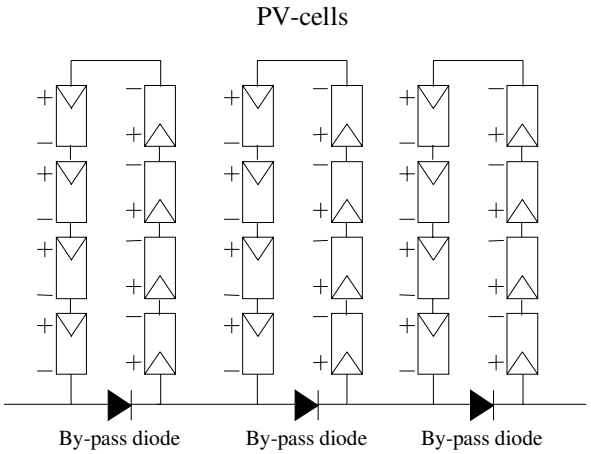

Figure 9. By-pass diodes for groups of eight cells.

2.4 Simulation of miss-match

To exemplify the impact of miss-match, some simulations are presented here. Matlab/Simulink is used as the tool and data are taken during a sunny day (1997-06-01) at Sankt Jörgen, Figure 10.

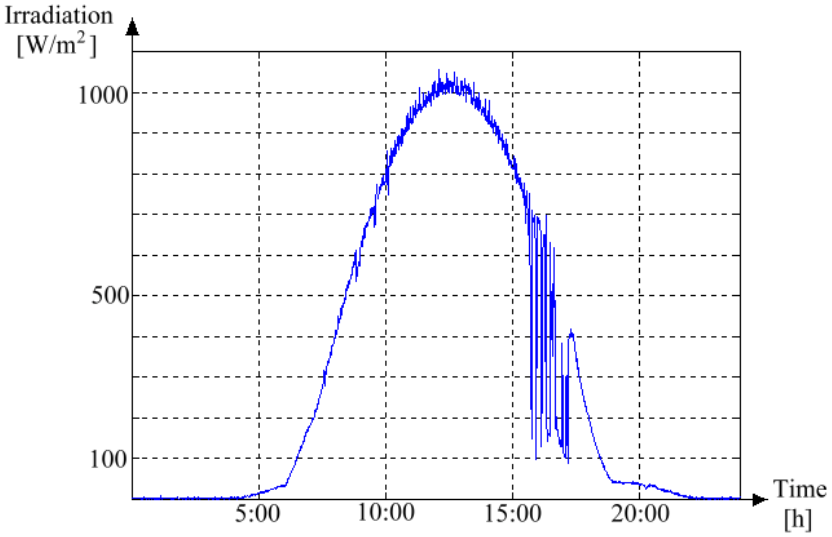

Figure 10. Irradiation at Sankt Jörgen 1997-06-01.

To model the PV-cells, the two-diode model is used and as the temperature dependency is not examined, the diode equation (1) is simplified to (3):

$$i_{diode} = C_{diode} \cdot T^{\frac{3}{n}} \cdot e^{-\frac{qU_g}{nkT}} \left(e^{\frac{qU_{diode}}{nkT}} - 1 \right) = I_{diode} \left(e^{\frac{U_{diode}}{nU_T}} - 1 \right) \qquad (3)$$

where

$$I_{diode} = C_{diode} \cdot T^{\frac{3}{n}} \cdot e^{-\frac{qU_g}{nkT}} \qquad (4)$$

and

$$U_T = \frac{kT}{q} \quad (5)$$

are constants. A least square method adapts the parameters to fit the iv-curve to the PV-cells at S:t Jörgen. The parameters are listed in Table 1 (Indices 1 and 2 refer to diode 1 and diode 2 in the two-diode model).

Table 1: The two-diode parameters used in the simulation.

Parameter	Value	Unit	Description
C_{ph}	3.7734e-3	m^2/V	Proportionality constant of generated photo current
I_{diode1}	5.1114e-12	A	diode 1 saturation current
n_1	1.0079		diode 1 ideality factor
I_{diode2}	3.8327e-05	A	diode 2 saturation current
n_2	2.0249		diode 2 ideality factor
R_s	9.9607e-04	Ω	solar cell series resistance
R_p	2.3733	Ω	solar cell shunt resistance

Furthermore, one cell out of 24 is supposed to be shaded at different degrees (0-100 %). In the case referred to as 'centralised', 24 PV-cells are connected in series and loaded by *one* central maximum power point tracker (MPPT), a device that continuously search for the MPP (more details in section 5.2). In the case referred to as 'decentralised', each PV-cell is loaded individually, see Figure 14.

The temperature dependence is not included. Neither are conversion losses considered, which give somewhat less favourable result for the decentralised system. The MPPT is implemented with a hill-climbing algorithm (described in Section 5.2) which takes current steps of 0.05 A, at a rate 10 times the input data resolution. This means that some small losses due to the imperfection of the MPPT are included, particularly when there are fast fluctuations in the irradiation as was the case on this particular afternoon.

In Figure 11, the energy production/dissipation by the shaded cell is shown when shaded from 0 % to 100 %.

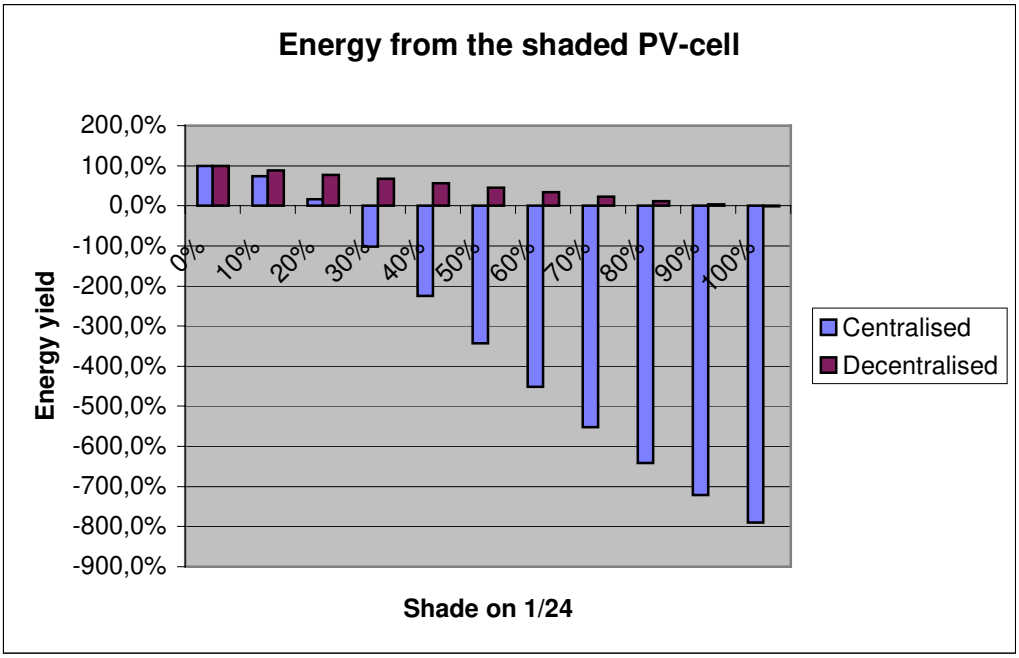

Figure 11. Energy production/consumption from a partly shaded PV-cell.

In the centralised system, the shaded PV-cell starts to dissipate power already when only less than 30 % of its surface is shaded, while the same shaded PV-cell in the decentralised system still produces approx. 70 % of the nominal value. In Figure 12, the miss-match effect is clearly seen as a decrease in energy yield from the non-shaded PV-cells when connected in series with the miss-matched PV-cell.

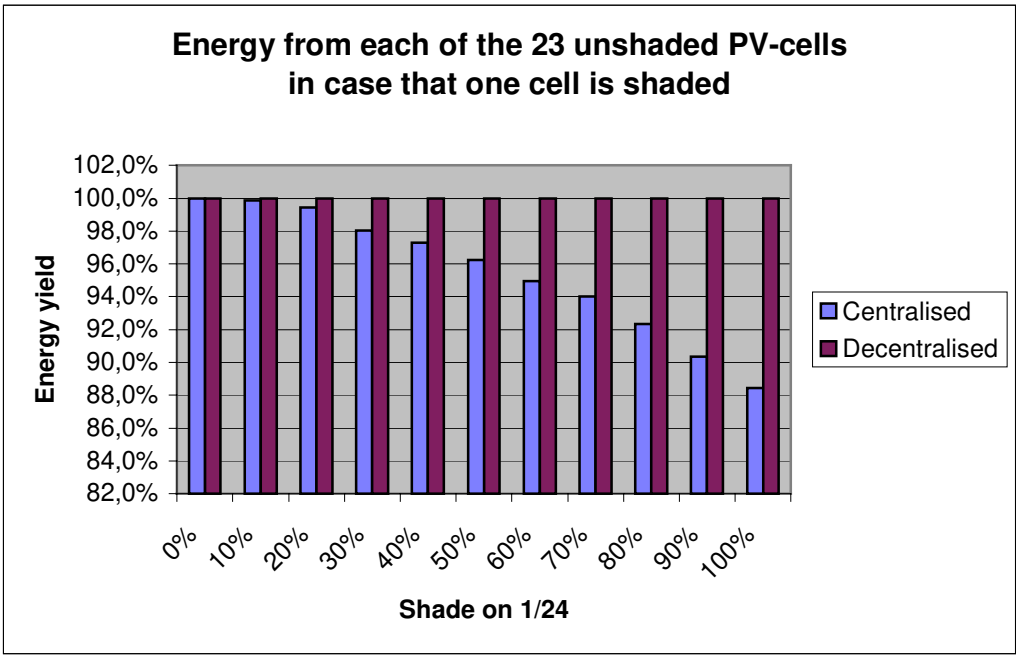

Figure 12. Energy production from non-shaded PV-cells in case one cell is shaded.

Since the PV-cells work independently in the decentralised system, the non-shaded PV-cells will always produce the rated power. For the PV-cells in series with the shaded cell, i.e., the centralised system, the over-all MPP will not coincide with the individual MPPs

In Figure 13, the total loss is plotted for the centralised system and for the decentralised system.

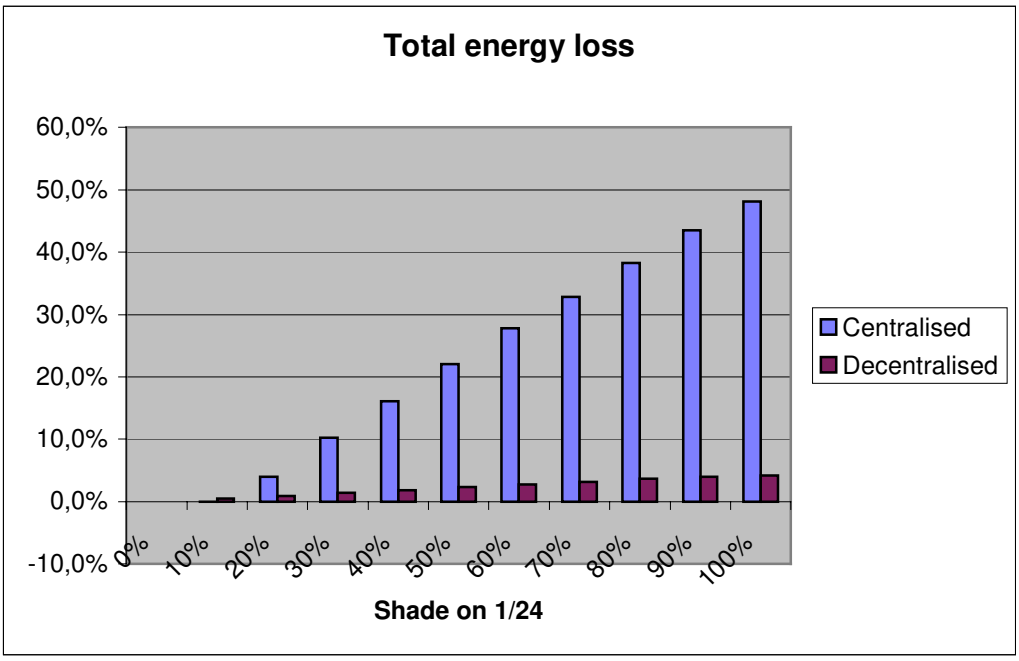

Figure 13. Total energy loss due to one partly shaded cell out of 24.

Miss-match losses in a decentralised system are limited to the shaded subsystem and are in the worst case 4.2 % (1/24). For the centralised system, the shaded PV-cell also affects the non-shaded PV-cells. For the worst case the shaded cell consumes almost eight times, or 790 %, of the rated production power. The 23 non-shaded PV-cells will produce only 88.4 % of their potential production. Hence, the total produced power is

$$\frac{1}{24}\cdot(-790\%)+\frac{23}{24}\cdot 88.4\% = 51.8\%$$

3. Different System Configurations

The difference between a conventional (centralised) system configuration and a decentralised system is shown in Figure 14. In a centralised system, all photovoltaics are connected to one loading unit. In a decentralised system, several power inverters are employed.

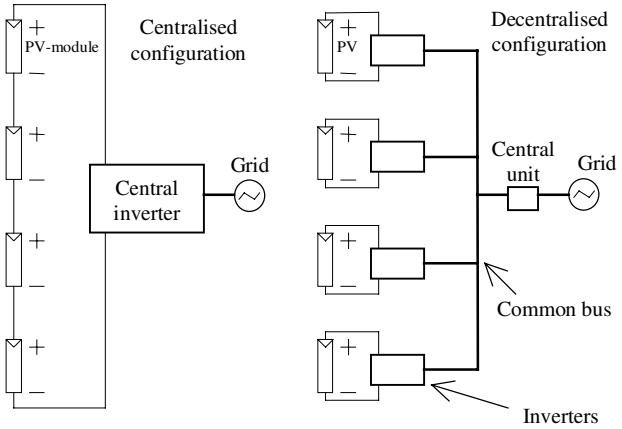

Figure 14. Centralised and decentralised configurations.

3.1 Conventional System with One Central Inverter

The conventional configuration for a PV-system is shown in Figure 15, where the PV-modules are connected in series to create a sufficiently high voltage. A full bridge-inverter transports the energy from the PV-generator to the grid. The inverter topology is a straightforward solution using as few components as possible. Using a central inverter gives a high efficiency and a low cost per watt.

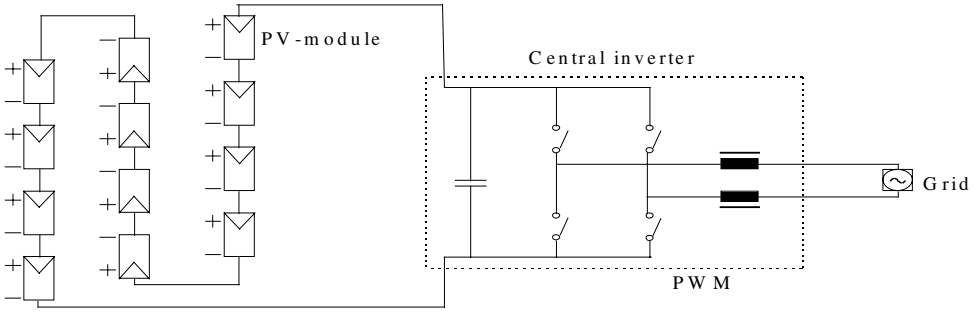

Figure 15. A full-bridge inverter using a large number of series connected PV-modules.

The disadvantages of this conventional topology are shading problems and no fault tolerance. As shown in the section, ‘Simulation of Miss-match’, this configuration is very sensitive to shading. Moreover, when using only one inverter, which occasionally trips, there is no energy production until the inverter is replaced or repaired.

3.2 String Inverters

The string inverter is a new concept on the market. Instead of a single inverter, several are employed in a PV-plant. They are of the order of 400-1000 W each and have an input voltage of approximately 100-400 V. The resulting PV-plant is a more fault-tolerant and more shade-tolerant system, in which each subsystem (string) is operated independently of the others. The units can often communicate with a supervisor, (a PC), which presents data and monitors their performance.

Figure 16. The south facade of the head office of Göteborg Energi.

An example is the 7 kW installation on the wall of the head-office of the power company, Göteborg Energi, installed in 1998 see Figure 16. The PV-modules (silicon thin-film) are arranged in seven groups, each connected to an inverter. The inverters Sunny Boy ™, 850 W and 700 W are from SWR, Germany.

3.3 Module Oriented Inverters

Small-scale inverters for integration with photovoltaic modules have recently been developed and introduced in the market [5][6][7]. They are even more shade-tolerant than string inverters. With such a system it is easier to expand existing installations. Furthermore, modular designs tend to be more fault-tolerant as the system still operates even if a single inverter fails. Two drawbacks of small-scale inverters are their higher cost and their lower efficiency. Although the cost of a small-scale inverter decreases with larger volumes, the cost per watt will still be higher due to the higher cost of, casing and connectors. However, since the cost of the inverter adds little to the overall cost of a PV-module, it can still be more cost-efficient to use decentralised inverters, as a higher energy yield can be obtained in locations where shade is present.

3.4 Cell Oriented Inverter

An interesting project is underway in Switzerland [10] where an inverter is developed for a single PV-cell with an input of approx. 1-2 V and 100 A. The advantage of this arrangement is that a miss-match between PV-cells no longer exists. If 15 % of the PV is shaded, the power production is only reduced by 15 %. The disadvantage is that it is extremely difficult to design a converter for such low input voltage and relatively high current. Inductances and resistances on the input side must be minimised and no conventional wiring is possible if reasonable efficiency is to be achieved. Even with an extreme design this system has difficulties in obtaining the same efficiency as a converter with higher voltage input.

4. Design of the System and the Main Circuit

In designing a power converter, a topology for the main circuit has to be chosen. As a second step, valves are selected based on the power, voltage and current the converter will be required at the same time minimising power dissipation and cost. The design and optimisation of magnetic components are also important items.

4.1 Selection of Configuration

A study of nine feasible configurations including converter topologies was performed in 1998. The process of selecting the configuration having the most desirable features is described in **Paper B**. In Appendices B-D the theoretical loss models are treated.

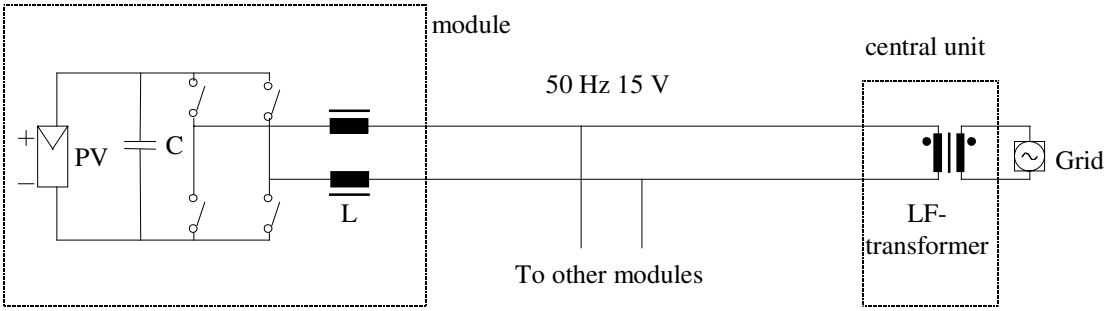

Figure 17. The selected decentralised configuration.

As a result of the study the configuration in Figure 17 with a low voltage AC-bus and decentralised inverters has been selected as a modification of the Sankt Jörgen PV-plant. It has a relatively high energy-efficiency and low cost, few components in the main circuit, which implies long mean time between failure and robustness. The central transformer can to some extent filter harmonics generated by the inverters.

Each inverter operates its PV-module at the maximum power point and feeds a sinusoidal current into the low voltage AC-bus. A one-phase- or a three-phase-transformer boosts the voltage up to the grid level of 230/400 V. The transformer can be considered to be very reliable, so the system becomes fault-tolerant as the modules work independently of each other. If one fails the others will keep on operating.

Some drawbacks of this configuration are relatively high currents in the bus, and the control circuit, the sensors and the power supply are somewhat more complex to realise as compared with DC-topologies. The topology has a minimum input voltage level, which together with the iv-cure for the PV-module sets limits to energy production at low irradiation. Also the input capacitor must be quite large to limit the 100 Hz ripple on the input voltage.

4.2 Design of the Main Circuit

To select the type of transistor to be used one can refer to the generalised diagram in Figure 18.

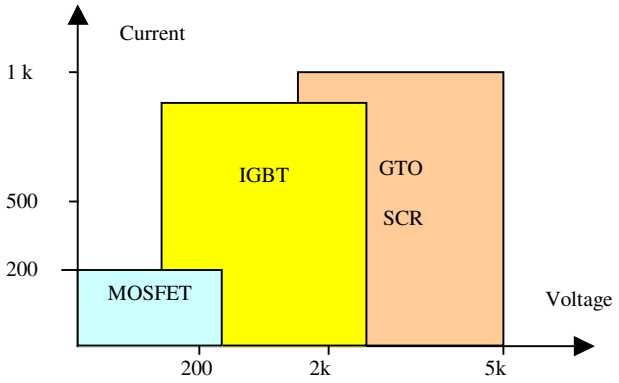

Figure 18. Different transistors are used at different power ranges.

For low power and low voltage applications the choice of switches is the MOSFET. The MOSFET has very low conducting losses (R_{DSon} of 8 mΩ available for 55 V, 100 A transistors) and is also easy to control which gives low switching losses. Additionally, it has a parasitic anti-parallel diode that can be used as a freewheel-diode. If this diode gives a poor performance (long reverse recovery time or high forward conducting voltage) external diodes, preferably schottky diodes could be used in parallel. The selected MOSFET HRF3205, has been tested with and without schottky diodes of the type: IR50SQ100. The difference was not measurable, so the diodes have been omitted.

The capacitance in the DC-link supplies the H-bridge with a stiff voltage. Its size is such that it will keep the 100 Hz ripple on the voltage within reasonable limits. When using a PV as the energy source, the ripple in the DC-link means that the working point of the iv-curve is not fixed but oscillates. In Appendix E, a theoretical derivation of the DC-link ripple and the current through the capacitance is given. In practice though the PV-source proved to be much stiffer in voltage than modelled due to the intrinsic capacitance in the PV-cells, and the actual ripple was found to be much less than calculated. A capacitance of 2200 µF gives a ripple of 3 % (worst-case).

The capacitor must also be able to carry a fairly high current, roughly 1.5-2 times the mean DC current. This maximum current is a significant parameter in selecting the capacitor. A low ESR (equivalent series resistance) is required for two reasons. Firstly the losses should be a minimum, secondly the ripple should be as low as possible.

The design of L is important, considering both power quality and efficiency. The core material together with the variation in flux density determines the iron losses (hysteresis and eddy currents). If the switching frequency is increased, the ripple losses will normally decrease (not for the fundamental though) but then the switch losses in the transistors will increase. A high inductance will also reduce the ripple current and, therefore, decrease the ripple losses but will, on the other hand, increase the conducting (copper) losses and, consequently, increase the weight and cost of the inductance. A selection of the inductance is made in the section on empirical data ‘Results and Measurements’.

5.The Analogue Controller, Prototype 1

The first prototype was built in spring of 1998. A classical analogue control was implemented with a proportional controller and triangular wave modulation.

The aim was to design a cheap inverter that can be mounted on the back of a PV-module and is easy to connect to the common bus. The voltage from the PV-modules used (GPV110M) is 25-50 V at a maximum power of 110 W. The AC-bus voltage was set to 15 V since its peak value must be lower than the minimum DC voltage.

5.1 An Analogue Controller Design

In Figure 19, the main circuit can be seen with current and voltage sensors on both the DC-side and the AC-side. The voltage potentials on the DC-side 'jumps' compared with the AC-side as the transistors are switched on and off. Therefore, signals between these sides need to be transferred via opto-couplers or signal transformers. Digital signals, such as the on/off signals to the transistor drive are easily realised, but a special analogue opto-coupler was used to measure the DC-current (linear opto-coupler in Figure 19). A 'LEM-module' could have done the job, but as the aim for the design was to make a cheap solution the expensive LEM-module was excluded.

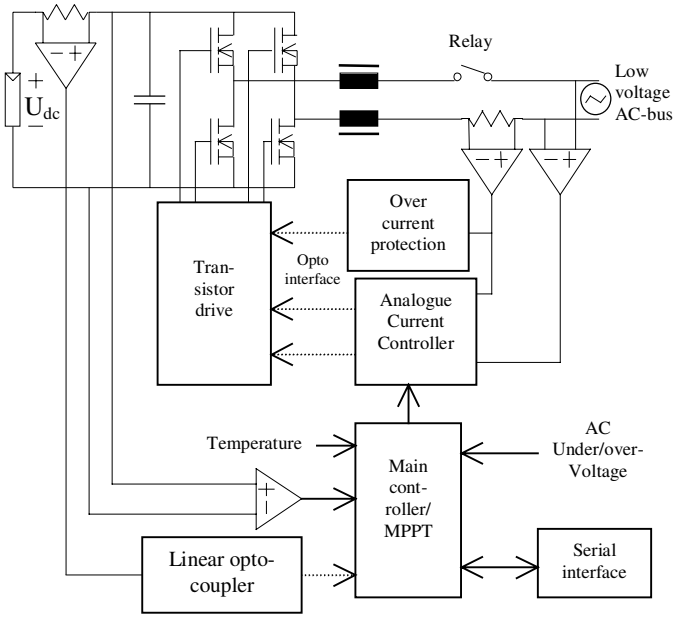

Figure 19. A block diagram of the main circuit and the controller.

The transistor drive converts the control signals to appropriate voltage levels for the transistors. It also inserts a delay time (blanking time) before switching on the transistors to prevent a short-circuit of the DC-link. The control signals are received via opto-couplers from the over current protection unit, which protects the transistors from too high current, and from the analogue controller. The analogue current controller shapes the output current and is described in the next paragraph. The main controller / MPPT gives directives to the current controller, and tries to find the MPP (as described in section 5.2). It also checks the voltage and frequency on the AC-bus and the temperature of the transistors. The main controller has a serial interface to report status to and receive its directives from a supervisor.

The principle of the analogue controller of the one-phase inverter is shown in Figure 20. It uses the grid-voltage, u_{grid}, as the wave shape generator for the current. u_{grid} is then multiplied by the mean current value, which is set by the micro controller, to obtain the current reference value, i_{ref}.

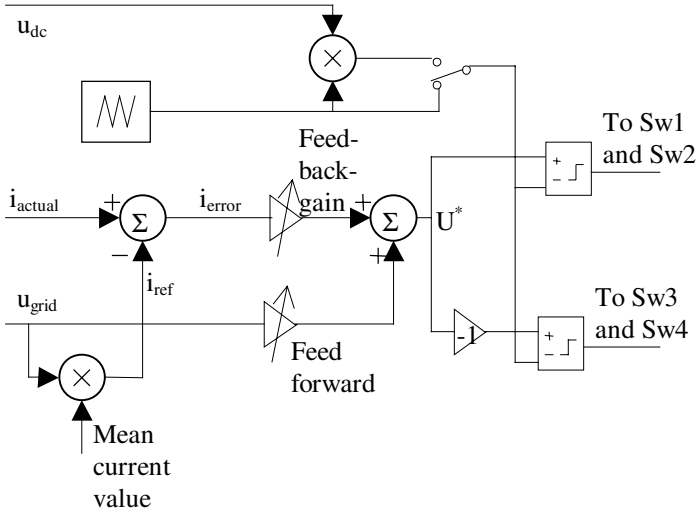

Figure 20. The analogue current controller and modulator.

By subtracting i_{ref} from the actual current, i_{actual}, an error signal is obtained i_{error}. A proportional-controller was realised by an amplifier with adjustable gain (P-parameter). The output-value from the amplifier, U*, represents the output voltage needed (actually the voltage-time-surface) to decrease i_{error}. This signal, U*, and its inverse are then compared with a triangular wave to generate the switch pattern to the transistors as seen in Figure 21. This is known as triangular wave-modulation.

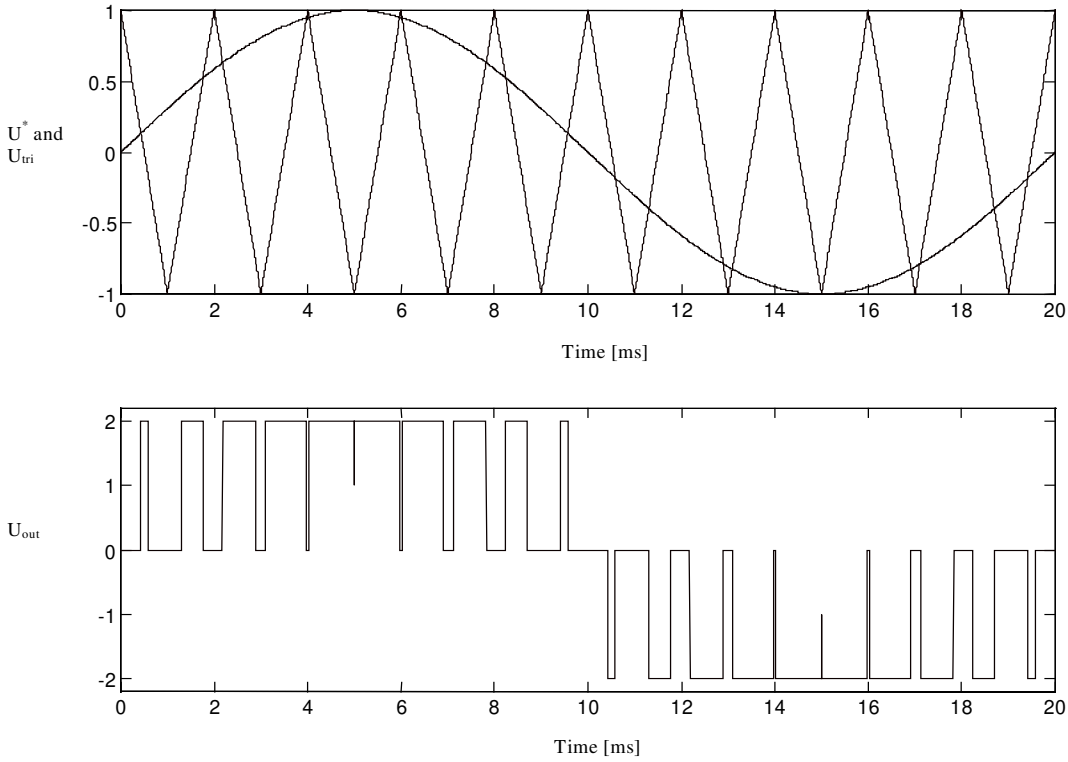

Figure 21. The switch pattern is generated from a triangular wave, U* and the inverse of it.

A feed-forward link was implemented to make the adjustment of the controller easier. The mean voltage from the H-bridge should equal the grid-voltage in phase and amplitude to get a zero current output. This forward link can be adjusted separately, with the feed-back-gain set to zero (i.e. no feedback). The feed-forward gain is then adjusted until zero current is obtained. Finally, the amplification in the feedback loop can be increased until proper performance is obtained i.e. until the output current follows the reference current without any oscillations due to a too large gain.

Another common feed-forward function often used is to scale the triangular-wave amplitude with the DC-link-voltage. This has the function of compensating a sagging DC-voltage with longer voltage-on times and makes the real voltage-time-surface out from the H-bridge linear to the output reference value, U*. In this case, where photovoltaic cells are used as a DC source, this feature is a disadvantage for the maximum power point tracker. The feed-forward will make the maximum power point less stable. When the DC-voltage starts to decrease, this feed-forward function will increase the voltage-on time, and thereby increase the current, which then causes the DC-voltage to decrease more, etc.

5.2 The maximum Power Point Tracker

To determine the maximum power point, an algorithm called hill-climbing was used. In theory this is an easy task. The load current is increased and the power is observed as it is increasing until 'the peak of the hill' is reached and the power starts to decrease. Then the current is being decreased and the power will increase again until 'the peak of the hill' is once again passed and it is time to start increasing the current again.

The maximum power point tracker was implemented using a fast 8-bit micro controller [11]. Due to the short distance between the power electronics and the sensitive analogue circuits and combined with a poor PCB-design, a lot of problems with noise were encountered.

After some modifications, such as shielded boxes and hardware- and software filters, it was possible to obtain good enough power values to implement the hill-climbing method.

5.3 Measurements

The prototype showed a good performance concerning the quality of the current injected to the grid due to a relatively high switching frequency of 22 kHz. Figure 22 shows an fast Fourier transform of the output current.

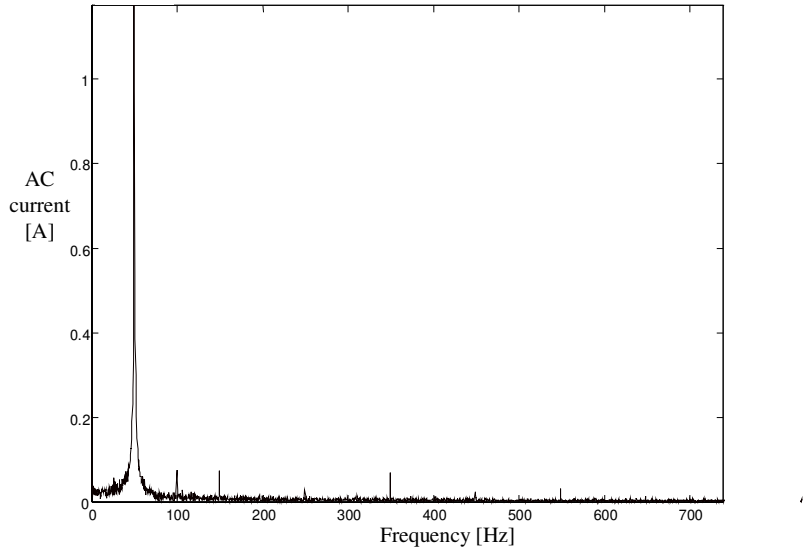

Figure 22. Frequency spectrum of the grid current.

The peak at 50 Hz has a value of about 2,5 A, peaks at 100Hz, 150Hz and 350Hz (the 2nd, 3rd and 7th harmonic) have a value of about 0,08A; that is 3.2% of the fundamental harmonic.

However, the inverter had a poor efficiency of around 60 %. This was probably due to the thin wire in the inductance and the high switching frequency. No further optimisation was performed for this prototype.

6. The Digital Controller, Prototype 2:

In 1999, the second generation of the PV-module-oriented inverter was designed and built. The main circuit was kept the same, while the controller was drastically changed.

6.1 Reasons for changing the Current Controller

There were several reasons for changing the design. During the development of Prototype 1, a lot of problems with noise were encountered. However, if a minimum of analogue circuits is used, noise problems can be minimised. An analogue design will always need extensive initial adjustments. Using a microprocessor control, the need for initial adjustments is minimised and the current control strategy can be changed or improved without any change in hardware. For instance, reactive power can be produced or consumed by changes in the programme. In Prototype 1, where the current reference is proportional to the grid voltage, reactive power was difficult to handle.

Another reason for changing the design was to reduce the number of components needed. Prototype 1 used four sensors; DC-voltage, DC-current, AC-voltage and AC-current. In the new design, only sensors for AC-current and DC-voltage are used, the possibility being that the latter may be superfluous.

The disadvantage of the new design is the limit in speed. If one wants to change the switching frequency in Prototype 1 only one capacitor had to be changed and the range could easily be up to 100 kHz (perhaps encountering some difficulties in the transistor drive with blanking times). For the microprocessor, even with hardware support, such as PWM-timers, signals must be converted to digital form, which takes time and a number of instructions must be executed for every control loop. The maximum estimated switching frequency for this new controller is approx. 20 kHz.

6.2 The Digital Controller – The use of Hysteresis Technique

The function of the digital design is described in **Paper C** which also contains measurements obtained from the current controller. Figure 23 clearly shows that two of the four sensors were removed (DC-current and AC-voltage).

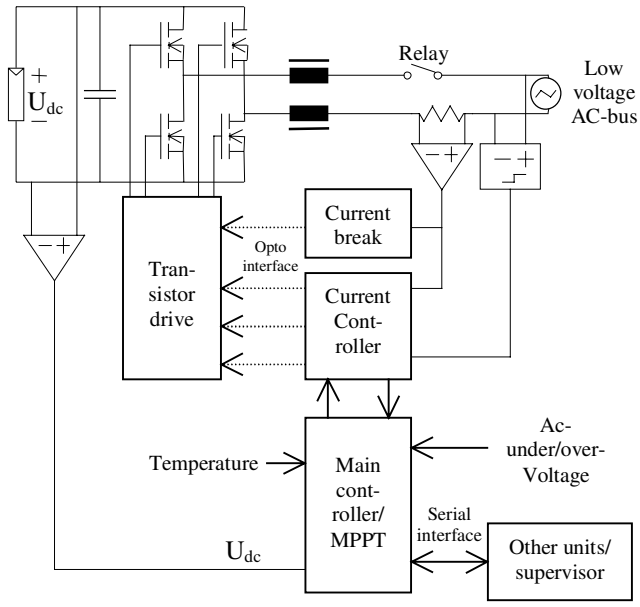

Figure 23. Block diagram of the inverter.

6.3 Change of the Inverter's Behaviour on the Grid

The change in control design fundamentally changes the inverter's behaviour on the grid.

The analogue controller made the inverter act as a 'negative resistive load'. The output current was proportional to the grid voltage. If there was distortion of the grid voltage, the produced current would be distorted as well. On the other hand, this behaviour is linear, so if some device on the grid tries to correct the distortion, the inverter does not introduce a non-linearity.

The digital controller generates a sinusoidal current to the grid, no matter what happens to the voltage. This controller will not produce distortions in the current to the grid even if there are fairly large distortions in grid voltage. On the other hand, the digital controller introduces a non-linearity between voltage and current, which could have a negative influence if another unit on the grid tries to improve the grid voltage shape.

7. Conclusions

Electricity produced by photovoltaics is a relative expensive technology and therefore it is important to optimise the use of the precious PV-modules. The impact of shading on photovoltaic power plants has shown to be important, as considerably energy losses can be the result of a poor design. Every possible measure should be taken to avoid shading but if it is inevitable, for instance, in urban locations, a decentralised energy conversion configuration should be employed. The subsystems work independently and only the sub-system shaded will be affected. This has the additional advantage of modular design making the system easy to maintain and expand.

Numerous alternative configurations are possible for a decentralised system, each with advantages and disadvantages. For grid connected systems without batteries or DC-loads, a low voltage AC-bus can be advantageous. The current conditioning is done locally by a full-bridge inverter, with low dissipation MOSFETs, and the voltage boost is done by a single transformer.

Experimental work has shown that it is possible to realise 110 W inverters with cheap components, which is a prerequisite to compete with centralised inverters. Measurements also confirm that a high efficiency of 93 % is achievable and a good power quality with a THD_i less than 8 % for all harmonics.

8. Future Work

Small scale inverters for photovoltaic applications have recently become a reality for making photovoltaic power plants more modular and more shade tolerant. However, they can probably never compete with centralised inverters in cost. Nevertheless, small scale inverters still have a great potential in cost reduction when produced in large series due to special designs using integrated control circuits and power switches with low requirements of cooling. The most expensive components are the capacitor and the inductance and therefore efforts to minimise or eliminate those are essential.

Most likely the different systems will co-exist in the future. For smaller applications where the shading situation is inevitable and particular for off-grid applications, small inverters or DC/DC-converters will reign while for larger photovoltaic power plants (>100 kW) larger inverters will transform the energy to the main grid.

What happens when hundreds or thousands of small inverters are connected to the main grid? And what happens when intermittent power generators, such as photovoltaics, can switch quickly from full energy production to none? These are questions that are important to further investigate when designing energy systems for the future.

9. References

[1] C. Reise, A. Kovach. “PV Shading Analysis in Complex Building Geometries”, Proceedings of the 13th European Photovoltaic Solar Energy Conference, Nice, 1995, pp. 575-579.

[2] A. Reinders et. al. “2250 PV-Roofs in Germany – Operating Results from Intensified Monitoring and Analysis through Numerical Modelling”, Proceedings of the 13th European Photovoltaic Solar Energy Conference, Nice, 1995, pp. 575-579.

[3] V. Quaschning and R. Hanitsch “Shading of Integrated Photovoltaic Systems in Buildings”, 4th European Conference SolarEnergy in Architecture and Urban Planing, Berlin, 26-29 March 1996.

[4] H. Oldenkamp, I. De Jong, “Next Generation of AC-module Inverters ”, Proceedings of the 2nd World Conference on Photovoltaic Solar Energy Conversion, Vienna, 1998, pp. 2078-2081.

[5] D. Schekulin et.al. “Module-integratable Inverters in the Power-range of 100-400 Watts”, Proceedings of the 13th European Photovoltaic Solar Energy Conference, Nice, 1995, pp. 1893-1896.

[6] M. Shafiyi, A. Louche “AC-modules for Autonomous and Grid Connected Applications”, Proceedings of the 13th European Photovoltaic Solar Energy Conference, Nice, 1995, pp. 1906-1909.

[7] W. Knaupp et.al. “Operation of a 10 kW Façade with 100 W AC Photovoltaic Modules”, 25th IEEE Photovoltaic Specialists Conference, Washington DC, 1996.

[8] V. Quaschning and R. Hanitsch “Numerical Simulation of Photovoltaic Generators with Shaded Cells”, 30th Universities Engineering Conference, Greenwich, Sept. 5-7, 1995, pp. 583-586

[9] "Semiconductor Physics and Devices" D. A. Neamen, Publisher Irwin 1992

[10] J. Riatsch, H. Stemmler and R. Schmidt, ”Single Cell Module Integrated Converter System for Photovoltaic Energy Generation”, Proceedings of the 7th European Conference on Power Electronics and Applications, Trondheim 1997.

[11] P. Holoch, "Control of Low-power Inverters for Photovoltaic Applications", Project report at Chalmers University of Technology, Department of Electric Power Engineering 1998.

Appendices

Appendix A: Control of the Full-bridge Inverter

A common way of arranging the switches in a power converter is the full-bridge, also called the H-bridge, as shown in Figure A.1. In this arrangement, both positive and negative voltages and currents can be applied to the load. The bridge can either be a voltage source inverter (VSI) or a current source inverter (CSI). In the first, and most common topology, the DC-link is voltage stiff, capacitive, and the load is current stiff, inductive. In a CSI it is the other way round. When the inverter is connected to the grid and a high quality of grid current is desired the VSI must be used. The CSI gives a square wave shaped grid current.

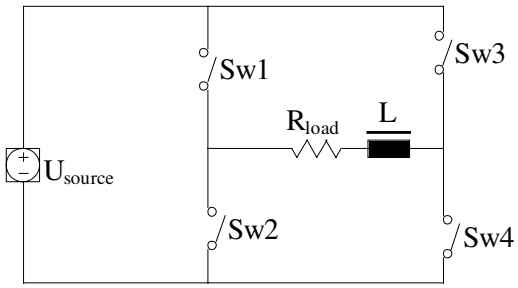

Figure A.1 A full bridge.

The H-bridge in Figure A.2 is connected to the grid and can apply $+U_{dc}$ (Sw1 and Sw4 on), $-U_{dc}$ (Sw2 and Sw3 on) or zero voltage (Sw1 and Sw3 on *or* Sw2 and Sw4 on) on the output, u_{out}. To force current into the AC-bus, U_{dc} must be higher than the peak value of the bus voltage to be able to create a sinusoidal current.

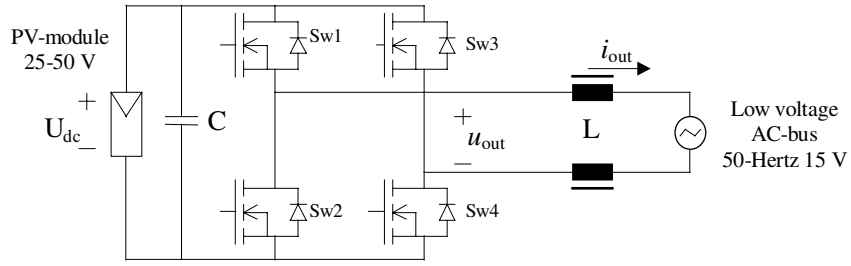

Figure A.2 The hull bridge working on the grid.

The circuit in Figure A.2 can be redrawn as Figure A.3, where the voltage source, U_{PWM}, represents the H-bridge and the DC-source. The two inductances are combined into one and the resistance in the inductor, wires, etc., has been explicitly shown.

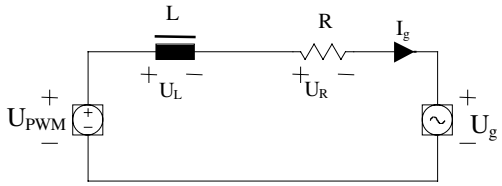

Figure A.3 A simplified scheme of the inverter.

It is now easy to construct a time-vector diagram of the required U_{PWM} to generate a sinusoidal current to the grid, provided the grid voltage, Ug, is sinusoidal and the components are linear. The vectors in Figure A.4 are the fundamental components of the voltages and currents. They rotate counter-clockwise at 50 Hertz.

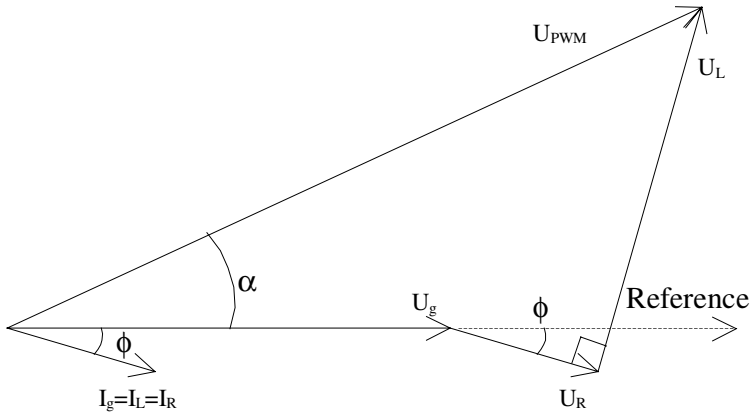

Figure A.4 Vector diagram of Figure A.3.

The phase shift, ϕ, represents the difference in phase for the grid current and the grid voltage. A positive ϕ, will make the inverter 'consume' reactive power while a negative ϕ, as in Figure A.4 will provide reactive power to the grid. For a PV-inverter, ϕ, is normally set to zero so only active power is produced at a minimum of loss. From Figure A.4, the following equations can be derived:

$$U_{PWM} = \sqrt{U_{PWM,X}^2 + U_{PWM,Y}^2}$$

$$\alpha = \arctan\frac{U_{PWM,Y}}{U_{PWM,X}}$$

where

$$U_{PWM,Y} = -U_R \sin\phi + U_L \cos\phi = -I_g R \sin\phi + I_g \omega L \cos\phi$$

$$U_{PWM,X} = U_g + U_R \cos\phi + U_L \sin\phi = U_g + I_g R \cos\phi + I_g \omega L \sin\phi$$

In other words, the H-bridge should be controlled to generate an average voltage of the magnitude; U_{PWM} and precede the grid voltage, Ug, by an angle α in time by combining the three possible output voltages.

Appendix B: Approximation for switch losses in MOSFET

A MOSFET-transistor in a switched application, changes state between on-state (low power dissipation) and off-state (no power dissipation), repetitively. In-between these two states the linear region lies where the MOSFET behaves as a voltage controlled current generator. In this region, the power dissipation is considerable, even though the switching transition is performed within approx.50-200 ns.

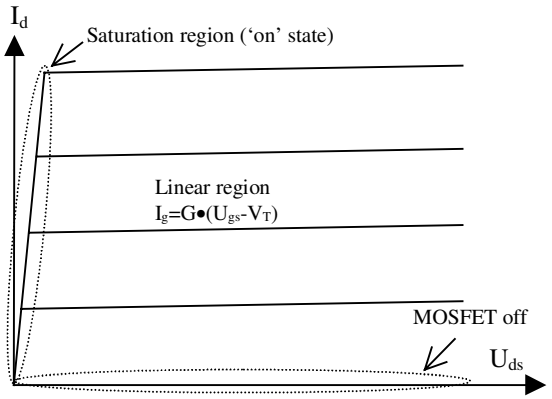

Figure B.1 IV-curves of a MOSFET.

The MOSFET has intrinsic capacitances between gate and source and between gate and drain that must be considered during switch-on and switch-off.

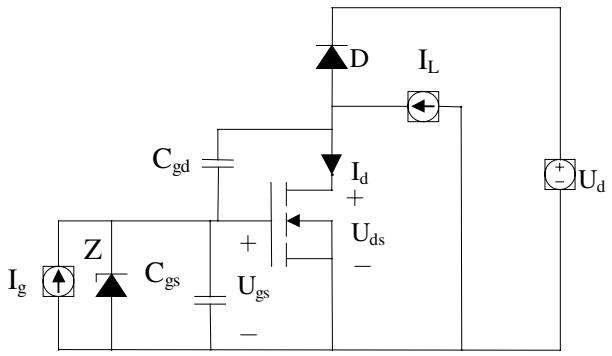

Figure B.2 Circuit for modelling a switch transition.

For commutating the current I_L from the diode D to the MOSFET, the following assumption is made. A current source applies a constant current I_g to the gate until the commutation is completed, see Figure B.3. In reality, the gate is normally controlled by a voltage source with a resistor in series. The resulting transition is, however, similar.

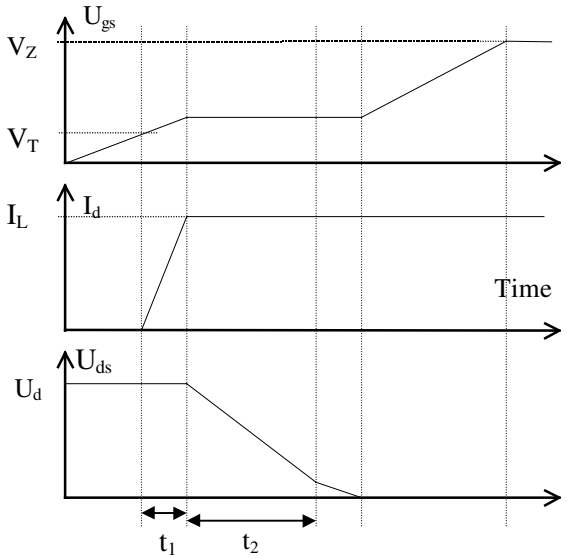

Figure B.3 A switch-on transition.

The MOSFET is off until U_{gs} equals the threshold voltage, V_T. In the first part of the linear region (during t_1), the slope of I_d (during t_1) is dependent on how fast C_{gs} in parallel with C_{dg} (C_{gs} dominating) is charged by I_g. In the second part of the linear region (during t_2), U_g is clamped by the constant drain current, I_d, and the transconductance G. The MOSFET conducts I_L and the voltage U_{ds} slope decreases due to I_g discharging C_{gd}.

The tail (after t_2) has another derivative due to the changed value of C_{gd} when the voltage U_{dg} changes sign. This happens at the gate voltage which is small compared to U_d and here the tail is neglected.

The energy dissipation during this ON-transition can be approximated by

$$E_{ON} = \frac{I_L U_d}{2} t_1 + \frac{I_L U_d}{2} t_2 = \frac{I_L U_d}{2} \cdot \left(t_1 + t_2\right) \approx \frac{I_L U_d}{2} t_{sw}$$

Actually, t_1 is dependent on I_L but since t_2 dominates, (t_1+t_2) can be treated as a constant switching time, t_{sw} , for all currents.

If the OFF-transition is treated equally at a switching frequency of, f_{sw}, the switch loss for one MOSFET will be simplified to

$$P_{sw} = 2 f_{sw} E_{ON} = f_{sw} t_{sw} I_L U_d$$

Appendix C: Losses for an H-bridge

A VSI H-bridge, Figure C.1, which is controlled in a three-state output manner,

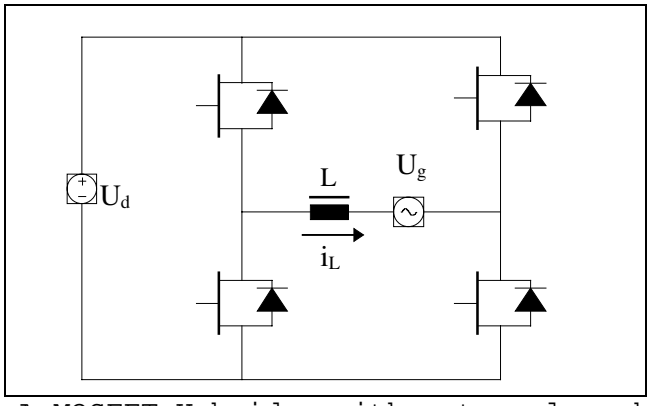

Figure C.1 A MOSFET H-bridge with external or body diodes.

will have a switching scheme which alternatively commutates the load current, i_L, from a transistor to a diode and then back to the transistor. D represents the duty cycle and is $0 < D < 1$.

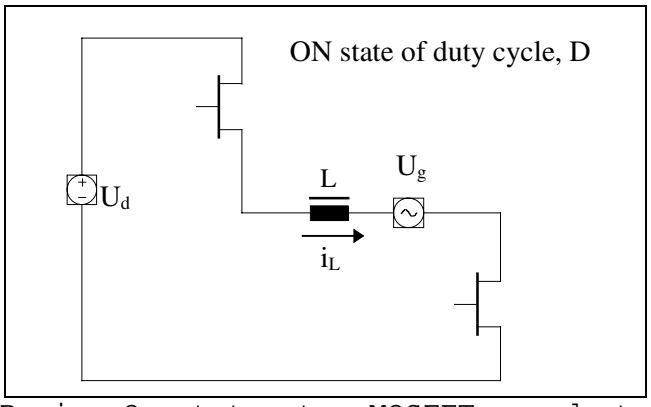

Figure C.2 During On state, two MOSFETs conduct the current.

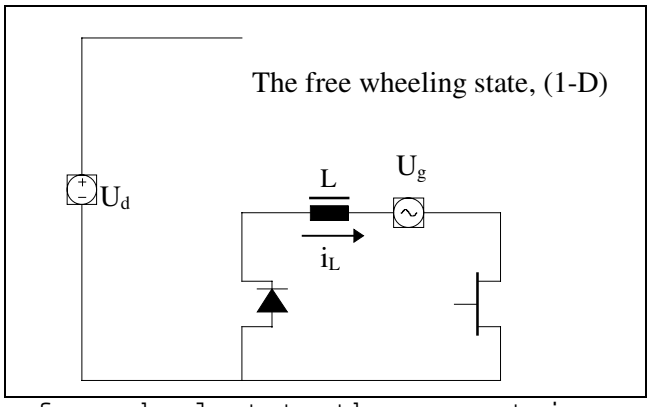

Figure C.3 During free wheel state the current is conducted by a diode and a MOSFET.

From Figures C.2 and C.3 the conclusion is that one diode conducts for (1-D) of the period while one transistor conducts throughout the cycle and additionally one conducts during D. Assuming that we can control the inverter to produce a sinusoidal current:

$$i_L(t) = \sqrt{2} I \cdot \sin(\omega t)$$

gives the required duty cycle

$$D(t) = Q \cdot \sin(\omega t + \alpha)$$

where

$$Q = \frac{\sqrt{2}}{U_d} \cdot \sqrt{U_g^2 + U_L^2} = \frac{\sqrt{2} U_g \sqrt{1 + \left(\frac{I}{I_{\max}} X_{L,pu} \right)^2}}{U_d} \approx \frac{\sqrt{2} U_g}{U_d}$$

$$\alpha = \arctan\left(\frac{U_L}{U_g} \right) = \arctan\left(\frac{I}{I_{\max}} X_{L,pu} \right) \approx 0$$

since $X_{L,pu}$ is small, in the order of 0.05-0.1

$$i_{diode}(t) = i_L(t) \cdot (1 - D(t)) = \sqrt{2} I \sin(\omega t) \cdot \left(1 - Q \sin(\omega t + \alpha)\right)$$
$$i_{transistor}(t) = i_L(t) \cdot D(t) = \sqrt{2} I \sin(\omega t) \cdot Q \sin(\omega t + \alpha)$$

The diode average current becomes:

$$I_{diode,AV} = \frac{1}{T/2} \int_{T/2} i_{diode} dt = \frac{1}{\pi} \int_0^{\pi} \sqrt{2} I \sin(\beta) \cdot \left(1 - Q \sin\left(\beta + \alpha\right)\right) d\beta \approx [\alpha small] \approx$$

$$\approx \frac{\sqrt{2} I}{\pi} \int_0^{\pi} \sin\beta - Q \sin^2 \beta d\beta = \frac{\sqrt{2} I}{\pi} \left(2 - \frac{\pi}{2} Q \right)$$

and the RMS-value (squared):

$$I_{diode,RMS}^2 = \frac{1}{T/2} \int_{T/2} i_{diode}^2 dt = \frac{1}{\pi} \int_0^{\pi} 2 I^2 \sin^2(\beta) \cdot \left(1 - Q \sin\left(\beta + \alpha\right)\right)^2 d\beta \approx [\alpha small] \approx$$

$$\approx \frac{2 I^2}{\pi} \int_0^{\pi} \sin^2 \beta - 2Q \sin^3 \beta + Q^2 \sin^4 \beta d\beta = \frac{2 I^2}{\pi} \left(\frac{\pi}{2} - 2Q \frac{4}{3} + Q^2 \frac{3\pi}{8} \right) = I^2 \left(1 - \frac{16}{3\pi} Q + \frac{3}{4} Q^2 \right)$$

For the MOSFET, which is resistive in the conducting state, we only need the RMS current (also squared):

$$I_{transistor,RMS}^2 = \frac{1}{T/2} \int_{T/2} i_{transistor}^2 dt = \frac{1}{\pi} \int_0^{\pi} 2 I^2 \sin^2(\beta) \cdot \left(Q \sin\left(\beta + \alpha\right)\right)^2 d\beta \approx [\alpha small] \approx$$

$$\approx \frac{2 I^2 Q^2}{\pi} \int_0^{\pi} \sin^4 \beta d\beta = \frac{2 I^2 Q^2}{\pi} \cdot \frac{3\pi}{8} = \frac{3Q^2}{4} I^2$$

Switch losses for the switching transistor (from appendix B)

$$P_{transistor,sw} = \frac{1}{T/2} \int_{T/2} f_{sw} t_{sw} U_d i(t) dt = \frac{f_{sw} t_{sw} U_d}{\pi} \int_0^{\pi} \sqrt{2} I \sin\beta d\beta = \frac{2\sqrt{2}}{\pi} f_{sw} t_{sw} U_d I$$

Switching losses for the diodes are neglected since they have no large voltage and current at the same time, however, this is not true in reality. The reverse recovery current at turn-off will contribute somewhat.

Finally, the losses of the switches for an H-bridge are:

$$P_{diodes,Cond} = V_d I_{diode,AV} + r_d I_{diode,RMS}^2 = V_d I\sqrt{2}\left(\frac{2}{\pi} - \frac{Q}{2}\right) + r_d I^2\left(1 - \frac{16}{3\pi}Q + \frac{3}{4}Q^2\right)$$

$$P_{transistors,Cond} = r_{DSon} I^2 + r_{DSon} I_{transistor,RMS}^2 = r_{DSon} I^2\left(1 + \frac{3}{4}Q^2\right)$$

$$P_{transistors,sw} = \frac{2\sqrt{2}}{\pi} f_{sw} t_{sw} U_{dc} I$$

$$P_{diodes,sw} = 0$$

Appendix D: Loss models for Transformers and Inductance

The assumed power loss model for magnetic components usually can be taken as the sum of a constant, (C1), and a term that has quadratic dependency on the current.

$$P_{loss} = C_1 + C_2 \cdot I^2$$

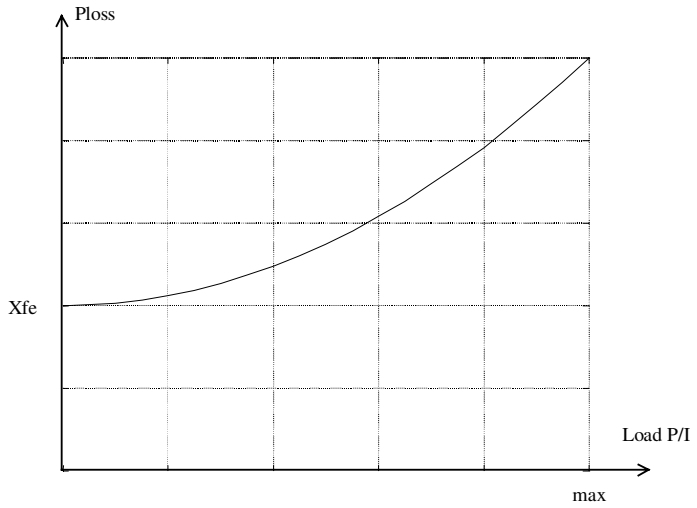

Figure D.1

As the current is proportional to the power at constant (grid) voltage we now obtain the following formula

$$P_{loss} = P_{\max}(1-\eta)\left(\frac{(1-X_{fe})}{I_{\max}^2}\cdot I^2 + X_{fe}\right) = P_{\max}(1-\eta)\left(\frac{(1-X_{fe})}{P_{\max}^2}\cdot P^2 + X_{fe}\right)$$

where X_{fe} is the fraction constant loss and η is the 'efficiency' at rated power.

Appendix E: Analysis of Currents and Voltages for the DC-capacitor

The H-bridge can be simplified as given in Figure E.1

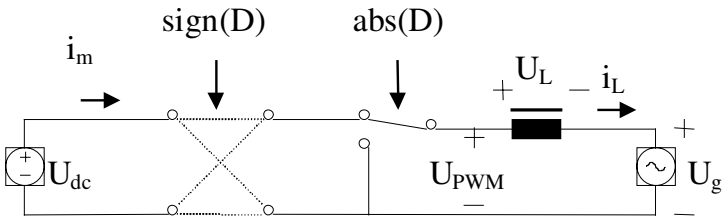

Figure E.1

U_{dc} is the DC source and it is switched to the grid filter to create a sinusoidal current, i_L. We allow the duty cycle, D to be $-1 \le D \le 1$. Here the sign determines the polarity and its absolute value is the relative time the DC-side is applied to the AC-side. The mean current i_m, from the DC source is noted:

$$i_m(t) = D(t) \cdot i_L(t)$$

and the mean voltage u_{PWM}:

$$u_{PWM}(t) = D(t) \cdot U_{dc}$$

If pure active power is desirable, i_L should be in phase with the grid voltage, u_g, see Figure E.2.

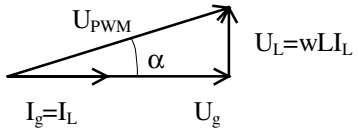

Figure E.2

$$u_g(t) = \sqrt{2} U_g \sin(\omega t)$$
$$i_L(t) = i_g(t) = \sqrt{2} \cdot I_L \sin(\omega t)$$
$$u_{PWM}(t) = \sqrt{2} \cdot U_{PWM} \sin(\alpha + \omega t) = \sqrt{2\left(U_g^2 + U_L^2\right)} \sin(\alpha + \omega t)$$

Now we have enough background to study the voltage and the current in the DC capacitor, see Figure E.3.

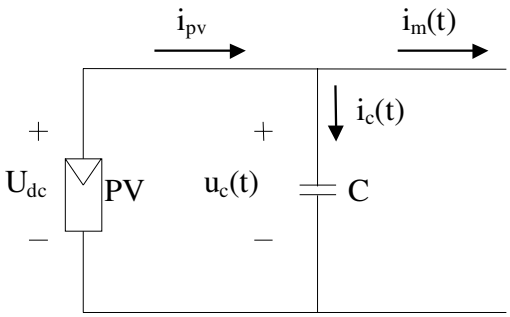

Figure E.3

From the previous equations and assuming that u_c does not vary too much and that the efficiency of the inverter is fairly high, i_m can be expressed:

$$i_m(t) = D \cdot i_L \approx [u_c = U_{dc} \approx Const.][I_{pv} U_{dc} \approx I_g U_g] \approx$$
$$\approx 2 I_{pv} A \sin(\omega t)\sin(\alpha + \omega t) = I_{pv} A[\cos\alpha - \cos(2\omega t + \alpha)]$$

where

$$A = \sqrt{1 + \left(\frac{U_{pv} I_{pv} \omega L}{U_g^2}\right)^2}$$

$$\alpha = \arctan\left(\frac{U_{pv} I_{pv} \omega L}{U_g^2}\right)$$

At a working point, U_{dc}, the I_{pv} of the PV source on the curve can be assumed to be linear around the working point, Figure E.4. This can be done by substituting the PV source with a voltage source, E, and a resistor, R, as in Figure E.5. The working point is defined by I_{pv}, U_{dc} and R from the iv-curve of a specific PV.

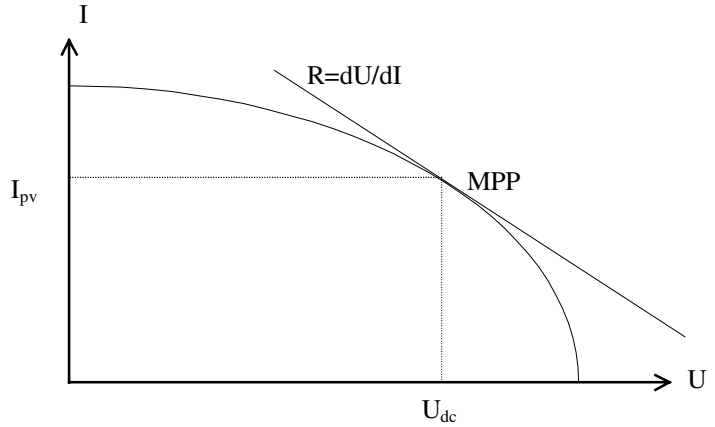

Figure E.4

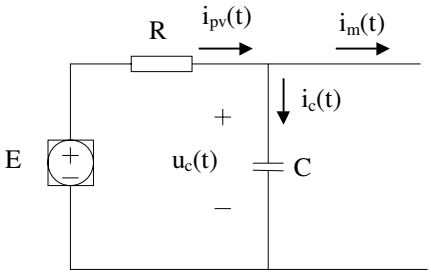

Figure E.5

From Figure E.5, the following three equations are derived.

$$i_c(t) = C\frac{du_c(t)}{dt}$$
$$i_{pv}(t) = i_c(t) + i_m(t)$$
$$E = Ri_{pv}(t) + u_c(t)$$

which together form the differential equation

$$\frac{du_c(t)}{dt} + \frac{1}{\tau}u_c(t) = \frac{E}{\tau} - \frac{i_m(t)}{C} = \frac{E}{\tau} - \frac{I_{pv}A}{C}\left[\cos\alpha - \cos(2\omega t - \alpha)\right]$$

where

$$\tau = RC$$

The general solution to this ordinary differential equation is

$$u_c(t) = u_c^h(t) + u_c^p(t)$$
$$u_c^h(t) = Be^{-\frac{t}{\tau}}$$
$$u_c^p(t) = C_1 + C_2\sin(2\omega t + \alpha) + C_3\cos(2\omega t + \alpha)$$

identifying C_1,C_2 and C_3 gives

$$C_1 = E - I_{pv}RA\cos\alpha$$
$$C_2 = 2\omega\tau C_3$$
$$C_3 = \frac{I_{pv}RA}{1+2\omega^2\tau^2}$$

where B is given by the boundary conditions at steady state,

$$u_c(0) = u_c(T) = u_c\left(\frac{\pi}{\omega}\right) \Rightarrow B = 0$$

To determine E we have the conditions at an average voltage

$$U_{dc} = \frac{1}{T}\int_0^T u_c(t)dt =$$

$$= \frac{1}{T}\int_0^T \left\{ E + I_{pv}RA\left[-\cos\alpha + \frac{2\omega\tau}{1+2\omega^2\tau^2}\sin(2\omega t+\alpha) + \frac{1}{1+2\omega^2\tau^2}\cos(2\omega t+\alpha)\right]\right\} dt =$$

$$= E - I_{pv}RA\cos\alpha$$

i.e.

$$E = U_{dc} + I_{pv}RA\cos\alpha$$

finally

$$u_c(t) = U_{pv} + \frac{I_{pv}R}{1+2\omega^2\tau^2}\sqrt{1+X_{L,pu}^2}\{2\omega\tau\sin(2\omega t+\alpha)+\cos(2\omega t+\alpha)\} =$$

$$= U_{pv} + \frac{I_{pv}R\sqrt{1+4\omega^2\tau^2}}{1+2\omega^2\tau^2}\sqrt{1+X_{L,pu}^2}\sin(2\omega t+\alpha+\varphi)$$

and

$$i_c(t) = C\frac{du_c}{dt} = \frac{2\omega\tau I_{pv}}{1+2\omega^2\tau^2}\sqrt{1+X_{L,pu}^2}\{2\omega\tau\cos(2\omega t+\alpha)-\sin(2\omega t+\alpha)\} =$$

$$= \frac{2\omega\tau I_{pv}}{1+2\omega^2\tau^2}\sqrt{1+X_{L,pu}^2}\cdot\sqrt{1+(2\omega\tau)^2}\sin(2\omega t+\theta)$$

Now, examine the actual PWM current

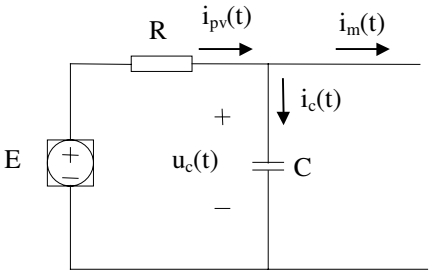

Figure E.6

where i_m during one switch cycle is approximated by a rectangle, Figure E.7, with a peak value of î

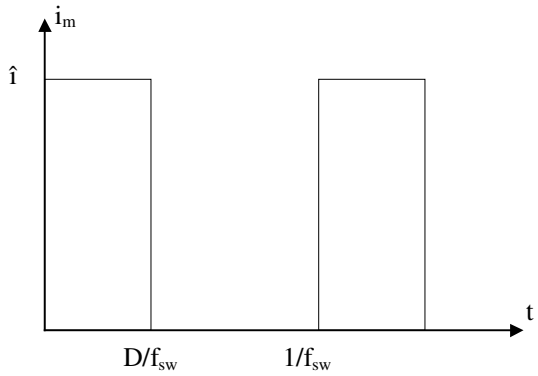

Figure E.7

$0 < D < 1$

$$\frac{d}{dt}u_c(t) + \frac{1}{\tau}u_c(t) = \left\{ \begin{array}{c} \frac{E}{\tau} - \frac{\hat{i}}{C} \\ \frac{E}{\tau} \end{array} \right\} \left\{ \begin{array}{c} 0 < t < \frac{D}{f_{sw}} \\ \frac{D}{f_{sw}} < t < \frac{1}{f_{sw}} \end{array} \right\}$$

$\tau = RC$

We have then two functions to solve per switch period

$$u_{c1}(t) = \hat{i}RF_1 e^{-\frac{t}{\tau}} + E - \hat{i}R$$

$$u_{c2}(t) = -\hat{i}RF_2 e^{-\frac{t}{\tau}} + E$$

To determine the constants F_1 and F_2 we need the boundary conditions for continuous voltage over the capacitor:

$$u_{c1}\left(\frac{D}{f_{sw}}\right) = u_{c2}\left(\frac{D}{f_{sw}}\right)$$

$$u_{c1}(0) = u_{c2}\left(\frac{1}{f_{sw}}\right)$$

which gives:

$$F_1 = \frac{\left(1 - e^{-\frac{1-D}{f_{sw}\tau}}\right)}{\left(1 - e^{-\frac{1}{f_{sw}\tau}}\right)}$$

$$F_2 = \frac{\left(e^{\frac{D}{f_{sw}\tau}} - 1\right)}{\left(1 - e^{-\frac{1}{f_{sw}\tau}}\right)}$$

and using

$$i_c = C\frac{du_c}{dt}$$

the currents are

$$i_{c1}(t) = -\hat{i}F_1 e^{-\frac{t}{\tau}}$$

$$i_{c2}(t) = \hat{i}F_2 e^{-\frac{t}{\tau}}$$

Finally, the RMS value can be calculated

$$I_{RMS} = \sqrt{\frac{1}{T}\int_T i_c^2 dt} = \sqrt{f_{sw}\left(\int_0^{\frac{D}{f_{sw}}} i_{c1}^2 dt + \int_{\frac{D}{f_{sw}}}^{\frac{1}{f_{sw}}} i_{c2}^2 dt\right)} =$$

$$= \sqrt{\frac{\hat{i}^2 f_{sw}\tau}{2}\left\{F_1^2 + \left(F_2^2 - F_1^2\right)e^{-\frac{2D}{f_{sw}\tau}} - F_2^2 e^{-\frac{2}{f_{sw}\tau}}\right\}}$$

Yield losses due to shading in a building-integrated PV installation; evaluation, simulation and suggestions for improvements

Per Carlsson and Dr. Lennart Cider, IVF, Argongatan 30, SE-431 53 Mölndal, Sweden,
Phone +46 31 706 6142, fax +46 31 27 61 30 e-mail pc@ivf.se
Björn Lindgren, Chalmers University of Technology, Department of Electric Power Engineering, SE-412 96 Gothenburg, SWEDEN
Phone +46 31 772 1641, Fax. +46 31 772 1633
E-mail: bjorn.lindgren@elkraft.chalmers.se

ABSTRACT: A planning tool has been developed for the effect of shading on yield for building-integrated PV installations. It is based on collecting local conditions by photographing the horizon with a Nikon small-image camera fitted with a panorama head and a special objective which has perspective correction. The tool also uses measurement of shading objects nearby, local solar irradiance and solar motion data as input data to existing software for estimating electricity production potential. Estimated electricity production potential is compared with the measured output produced from a shaded roof-mounted PV installation in Gothenburg in the west of Sweden. This method makes it possible to optimise or improve a PV installation from the point of view of shading, already at the planning stage.
KEY WORDS: yield, building-integrated photovoltaic, shading

1 INTRODUCTION

Experience gained in the German 1000-roof project shows that shading of solar cells is the largest loss factor. Shading of one cell limits the current in the entire module. For example, a partially shaded cell can reduce the yield by 70 % even though only 2% of the module is shaded. The problem is to be able to estimate in advance the electricity production that can be expected from a given of the solar cell installation. The solar cell installation at Sankt Jörgen Environmental Park serves as a reference installation for shading studies. The siting and design of this installation is not optimal as trees, a chimney and a ventilation fan casing shade the panels much of the day. In addition, the panels are also narrow spaced so they shade each other. This paper proposes a method for predicting the potential electricity production of shaded solar modules.

2 METHOD

The method involves acquiring the local horizon line with the aid of a special photography technique. Nearby objects or planned buildings are measured or computed. Data from the total shading situation is used in a program for calculating the available solar irradiance. The various steps for the reference installation at Sankt Jörgen are described below.

2.1 The PV roof installation

The roof installation is a part of the experimental solar energy installation at Sankt Jörgen;. Electricity produced is supplied partly to the grid and partly to a battery. The roof installation consists of three rows, with twelve GPV 110 modules in each, supplying electricity to the grid via a DC/AC converter. Twelve modules vertically mounted on a wall also supply the electricity to the same DC/AC converter. In each row and on the wall the twelve modules are connected in series. The modules have 72 cells in series with a nominell effect of 110 W. The

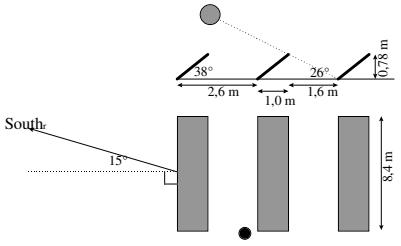

Figure 1 Schematic drawing of the roof panels

overall dimensions of the modules are 0.68 x 1.3 m including frame. Each module has three bypass diodes. With the upright orientation of the modules on the roof at Sankt Jörgen, the modules are divided vertically by the diodes. This means that a longitudinal shadow at the bottom edge shuts off all the modules in the row.

The panels are angled 38° from the horizontal plane. The distance between the rows of panels is 2.6 m (1.6 m from the rear edge to the next front edge). This means that the top edge of the panel in front shades the panel behind with a maximum elevation angle of 26°. The entire installation is directed 15° towards east from south.,See Figure 1.

2.2 Photographing the horizon line

The horizon line (360°) at Sankt Jörgen has been photographed. A special lens with perspective correction and a ‘panorama head’ were used. With perspective correction, an object can be photographed from the horizon upwards without the camera having to he aimed upwards and without distortion of the image. This is very well suited for photographing the horizon line where

Figure 2 The horisontal line photographed from the roof

only objects above the horizon are to be recorded. The lens used is a PC-Nikkor 28 mm on Nikon F-801s small-image camera. Eight images must be taken to photograph the entire horizon (360°). A single image covers just over 45° in width and early 40° in height. shows the eight images which represent the horizon line, taken from the eastern top edge of the front solar cell panel. The images overlap and need to be converted into horizontal and vertical degrees. The rotation from one image to the next is 45°. This is taken care of by a "panorama head" between the tripod and the camera. The panorama head used here was a Nikon AP-2. This has snap-in rotational positions and an integral level for accurate setting.

2.3 Digitising and calibrating the horizon line

At least one compass bearing from the camera position to a known point in the image series is needed to orient the entire image series for post-processing. It is also advisable to use an angle gauge to record a few vertical (elevation) angles, for example the highest and lowest points (°) on the horizon line. In this image series these are the chimney (28° elevation) and the horizon in the west (0° elevation). In post-processing, the images were scanned into an image processing program with coordinate handling. This makes processing easier. We used Paint Shop Pro. The coordinates are specified as shown in
The top left (x1,y1) and bottom right (x2,y2) coordinates are registered. The coordinates of the horizon line are registered and converted to centred coordinates (xx_i,yy_i) as follows $xx_i = \frac{x2 + x1}{2} - x$; $yy_i = (y2 - y)$;
where i is the image number.

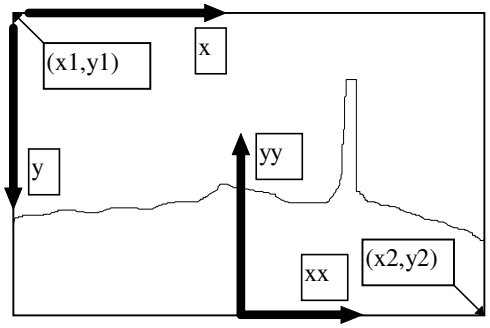

Figure 3 Coordinate system for one image in the series

To calculate the overlap between images, a number of points present on two adjacent images are identified as shown in Figure 4

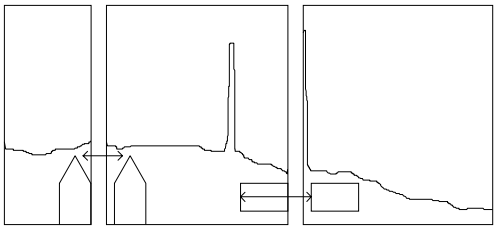

Figure 4 Identification of points that overlap

The coordinates (xx_i) are calculated as described above. The effect of the overlap can now be calculated numerically since the azimuth angle (a_s) must have the same value on two adjacent images, in accordance

$$a_s = \arctan\left(\frac{xx_i}{m}\right)\cdot(i\times 45°) =$$

$$= \arctan\left(\frac{xx_{i+1}}{m}\right)((i+1)\times 45°)$$

where m is a parameter

The parameter m takes account of the overlap between the images and makes the readings independent of any

enlargement of the image series. If several overlapping points are used, the parameter m can be determined with greater accuracy. One way of doing this is to use the least squares method.
The next step is to calculate elevations (vertical angles). The coordinates (xx_i,yy_i) of the lowest point and the highest point are matched to the readings (in degrees) as follows: $h = \arctan\left(\frac{yy_i - y_0}{\sqrt{(xx_i^2 + m^2)}}\right)$

where y_0 is a parameter

The parameter y_0 takes account of the fact that 0° elevation is not exactly at the bottom edge of the image. If there are several sets of measured elevations, y_0 can be adjusted using the least squares method. Finally the

azimuth (lateral) angle a_s is adjusted using at least one actual compass bearing a_k as follows:

$a_k = a_s - a_j$; where a_j is an adjustable parameter.

In this way, the three parameters m, y_0 and a_j are adjusted. The equivalents are derived trigonometrically on the basis of the distance from the camera position to the photographed objects. The accuracy of the method when determining the horizon line is of the order of 1° both in elevation and in azimuth.
Figure 5 shows converted values from a series of scanned images plotted on the same diagram.

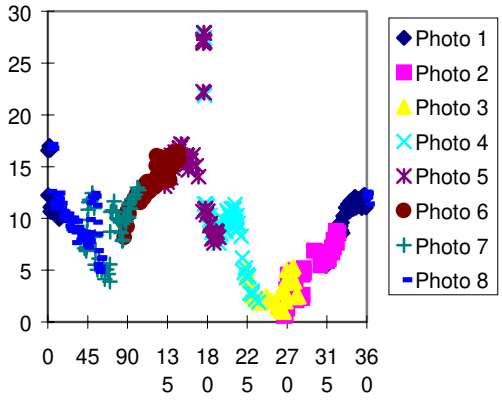

Figure 5 Horizon line calculated from image series at Sankt Jörgen

2.4 Data acquisition equipment

The data acquisition equipment at Sankt Jörgen is wired for separate metering of the output produced by the four panels. Figure shows the power produced by the three panels, P3 at the front, P2 in the middle and P1 at the back. The power (W) is calculated as P = U x I. The voltage is about 400 V and the current is up to 2 A. Ga is the reference cell, which shows the irradiance in W/m^2. It is evident from the readings obtained that panel P2 is shaded all morning by the ventilation fan casing, but the currents from the other two panels is also limited at solar insulation over 600W. Later, this was found to be due to a defect in the DC/AC converter.

2.5 Solar irradiance during the measurement period

Solar irradiance data for research purposes was ordered from the Swedish Meteorological and Hydrological Institute (SMHI). These were readings with a one-hour resolution from a measurement station in Gothenburg for the period January - October 1997. Having irradiance data from the same period allows comparison of simulation and collected PV data day by day.

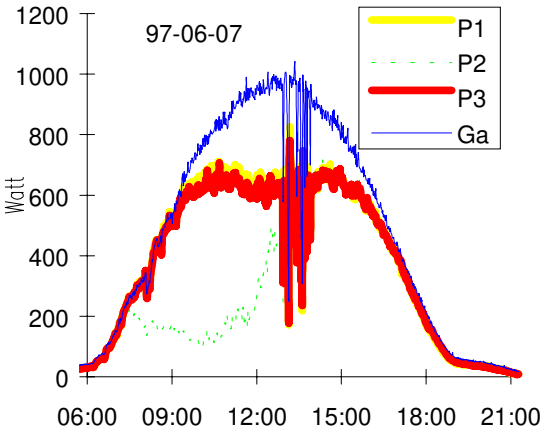

Figure 6 Power produced by the three solar panels

2.6 Simulation of incident irradiance on shaded solar cell panels

SUNDI [1] is a program that computes the irradiated power to a shaded surface. The program is an alternative to other significantly more computation-intensive programs such as Radiance. With SUNDI it is also possible to describe irregular shading objects as polynomials, a feature that we exploit here. The program needs the following data: global irradiance W/m^2 or direct irradiance and diffuse irradiance W/m^2 as time-resolved data with at least one value per hour; position of PV installation, longitude and latitude; lateral rotation from south and inclination to the plane of the PV module; albedo (ground reflection coefficient of irradiance, usually set at 0.2); and the horizon line (a,h), which are associated values of azimuth and elevation angles for shading. Output data is solar irradiance at a point on the tilted, shaded plane. The time resolution is the same as for input data. According to the designer of the program, the shaded point should be chosen with care. The most shaded point is regarded as the most suitable point to choose. In fact, SUNDI calculates the solar irradiance at a shaded point, but we transfer this to apply to the entire series-connected solar cell panel by analysing whether any part of the panel is shaded. When a single point is shaded, we apply this to the entire panel. For the front, least shaded panel, P3, this means that the chimney occupies 7° in azimuth instead of 3° as seen from one point. This will be an over-estimation of the shading, but it gives a far better estimation of the actual effect of shading than a linear model. When we contacted the program designer [2], he confirmed that this approach is possible and functional. If the installation is large, it may be advisable to register the horizon line at several points. Figure 7 shows a screen dump from SUNDI for the front panel. The diagram includes the computed horizon line, together with solar motion curves for Gothenburg. It is evident from the diagram that the sun does not reach the installation at all around the time of the winter solstice. From the beginning of October to the beginning of March, the chimney shades the panel for part of the day.

For the middle solar cell panel (P2) there are two additional shading objects, the ventilation fan casing and

the solar cell panel in front. Because of the ventilation fan casing, the sun does not reach the entire panel until the afternoon and only during the summer months, since the panel in front is also in the way.

The horizon line for panel P1 is produced in the same way. It differs from the horizon line for P2 because the ventilation fan casing is not involved, but apart from this they are identical. From September to March, the panel in front (P2) shades P1 in the morning. From the middle of October to the end of February, the sun does not reach the bottom of the panel at any time during the day.

Once the three horizon lines have been generated, the solar irradiance for the shaded panels can be simulated. The input data is the actual irradiance measured by SMHI. The SUNDI publication program gives results with the same time resolution as the input data. We therefore made each hourly mean value represent three instantaneous values: HH:00, HH:20 and HH:40. This improves the resolution of the shading calculations. Figure 8 shows the result of the calculations in a diagram. There is clear agreement between the simulated and the collected data, as shown by Figure 6. The most shaded panel, P2, follows the others up to around 7-8 o'clock, after which it loses production throughout the entire morning. When the shadow from the ventilation fan casing has passed, electricity production rises to the same order of magnitude as the other panels.

2.7 Video recording and ray trace simulation

A video recording of the PV installation was made on 13 October 1997, a sunny day, to record the way in which the fan casing, the solar panels and the chimney shade the installation and how the power produced is affected. A ray trace simulation of the shading [3] was done
to

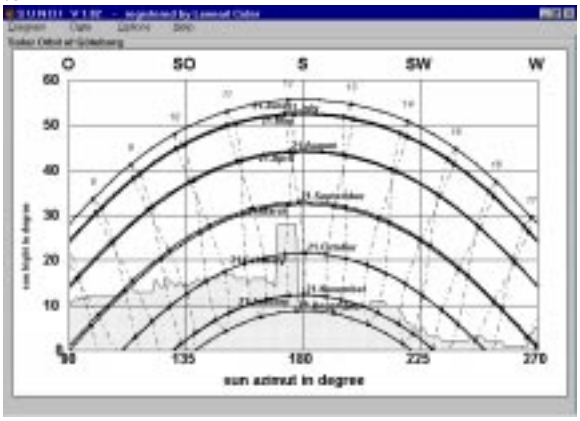

Figure 7 Horizon line and solar motion seen from the front panel (P3). Screen dump from SUNDI.

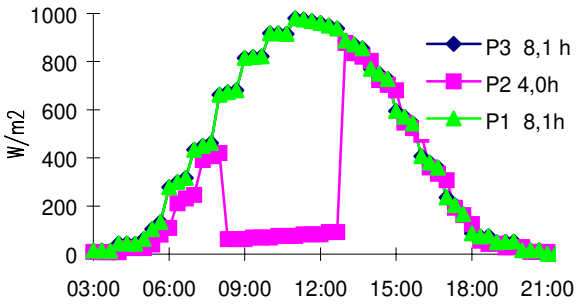

Figure 8 Simulation of shaded irradiance for one day (97-06-07)

compare both with the actual shading and the measured power produced. This simulation is based on the calculated solar orbit for the 13th of October, the dimensions and orientation of the installation, the loaded horizon line and the positions of nearby shading objects (fan casing and chimney.
A series of images showing the situation every four minutes (one degree of angular motion of the sun) has been produced. The components of the series are shown in Figure 9. Comparison: Ray trace simulation, video recording and electricity produced
An animation which can be run on a PC with media player has been produced. At 12:00 noon, the front panel (P3) is fully exposed from sunrise and produces just over 800 W. The two panels behind it give less than 50 W each because of partial shading. Between 12.32 and 13.00 the shadow of the chimney is wholly or partially over all the panels. The production of electricity is 50 W per panel. After 13.32 the shadows of the chimney and the fan casing have both passed. Panel P3 once again delivers 800 W, but at the bottom of panels P2 and P1 there still remains a slowly shrinking shadow from the panel in front.. The production of electricity by the shaded panels increases proportionately as the bottom row of cells begins to be illuminated. The degree of illumination of the most shaded cell determines the electricity production.

2.8 Simulated shaded solar irradiance - measured yield

During the 10 months (304 days) of the measurement period, the installation provided usable measurement data for 147 days. For three months (92 days) the installation was shut down because of damage at the beginning of March. The simulating shaded solar irradiance is obtained with SUNDI as described in section 2.6. Table 1 below lists both simulated and measured values in hours at a reference irradiance of 1000 W/m^2 and a nominal power of 110 W from each modul. In this way the values can be compared in pairs. The measured values include the electrical conversion losses, so they are naturally lower than the simulated values. During the summer months the most shaded panel (P2) produces about 30% less electricity than the other two (P1 and P2). In February and October, the front panel gives significantly more than the other two because of self-shading. Table 1 Comparison of simulated irradiance and measured yield

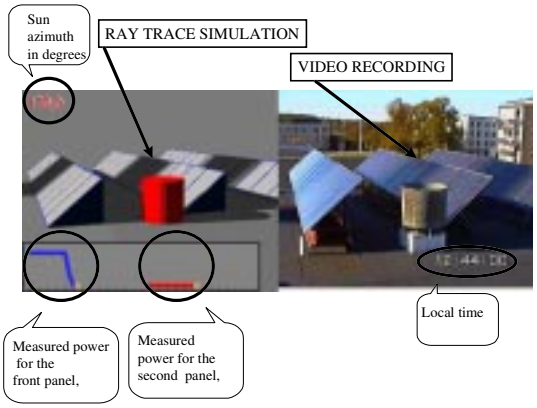

Figure 9 Comparison: Ray trace simulation, video recording and electricity produced

Table 1 Comparison of simulated irradiance and measured yield

	Simulated solar irradiance hours at reference irradiance			**Measured yield hours at nominal power**		
	P1	P2	P3	P1	P2	P3
February	7.0	4.9	14.6	5.1	4.8	10.3
June	133.9	75.1	138.8	84.9	66.9	83.8
July	174.5	88.4	179.9	113.4	79.2	111.0
August	147.0	74.7	151.1	90.5	63.2	88.5
September	84.0	39.3	89.0	25.5	19.8	25.7
October	14.6	10.2	39.1	11.5	11.3	32.9
Total:	560.9	292.6	612.5	330.9	245.3	352.2

The measured yields June through September are lower than the simulated yields mainly due to the defect DC/AC converter as seen in Figure 6. Other losses such as wiring and mismatch losses has not been accounted for in the simulated data.

However, there is a good day-by-day correlation between simulated and measured data (about 0.90).

3 Improving the existing installation

The proposed shading model can be used to predict the electricity production for a series of changes. The installation produced electricity for 309 hours as a mean value. The potential for the location is 1119 hours. Improvements could be achieved by reducing conversion losses, increasing availability, removing sources of shading, turning the panels, moving the panels further apart or equipping the installation with decentralised inverters.

4 DISCUSSION AND CONCLUSIONS

The shading model described gives us tools to work with, partly to improve an existing installation and partly to plan new installations on the basis of the effect of shading. The amount of electricity produced by the roof installation at Sankt Jörgen could be dramatically increased by implementing a number of the improvements suggested.
The proposed model is not an electrical simulation of the electricity production of the panels. As described here, the model overstates the effect of the shadowing. Since it is sensitive to shadowing it provides an opportunity to minimise the effect of shadowing at the planning stage.

A decentralised inverter/converter system can be achieved in many ways. The result is anyhow a considerably more shadow tolerant system where every subsystem maximise the yield from its PV-cells and the overall performance is increased. In building integrated PV-plants, where shadows are inevitable, these kind of systems should be considered.

3 ACKNOWLEDGEMENT

The Research Foundation at Göteborg Energi AB are gratefully acknowledged for their finical support

4 REFERENCES

1 Volker Quasching and Rolf Hantisch, Quick Determination of Irradiance Reduction Caused by Shading at PV-Locations, 13th European Photovoltaic Solar Energy Conference, 1995, pp 683-686.

2 Volker Quasching, Personal communication, 1997-09-17.

3 Peter Gustafsson, PSG Designdata, 1997-11-17.

Topology for Decentralised Solar Energy Inverters with a Low Voltage AC-Bus

Björn Lindgren
CHALMERS UNIVERSITY OF TECHNOLOGY
Department of Electrical Power Engineering
SE-412 96 Göteborg, Sweden
Phone +46-31-772 1641/Fax +46-31-772 1633
bjorn.lindgren@elkraft.chalmers.se
www.elkraft.chalmers.se

Acknowledgements

The Research Foundation at Göteborg Energi AB is gratefully acknowledged for its finical support.

Keywords

Renewable energy systems, Solar cell systems, Generation of electrical energy, Single phase systems, Efficiency, Reliability, Modelling, Design, Converter circuits, Control.

Abstract

The development of photovoltaic inverters has recently moved towards smaller units in order to increase modularity and energy yield in shaded areas. The drawbacks are higher cost, as well as lower efficiency in comparison with larger units. This paper compares eight decentralised configurations and one conventional, with respect to efficiency and cost. Reliability and personal safety are also considered. The pre-requisite is that standard PV-modules of 25-50 V, 110 W, are to be used and the energy is to be transformed to the national grid of 230 V, 50 Hz. The recommended configuration is a low voltage AC-bus, which can reduce costs while maintaining or improving efficiency and safety.

1 Introduction

Photovoltaics (PV), also called solar cells, have great potential to supply the world with energy with a minimum of impact on the environment. So far, the technique has been too expensive but governments all over the world have started up large projects to lower the price and gain more knowledge about photovoltaics.

Small-scale inverters for integration with photovoltaic modules have recently been developed and introduced onto the market [1]. The system becomes more shade-tolerant [2] and it is easier to expand existing installations compared with conventional systems with one central inverter. Furthermore, modular designs tend to be more fault-tolerant, as the system still operates even if one inverter fails. Two drawbacks of small-scale inverters are their higher cost and lower efficiency. Although the cost of a small-scale inverter decreases with larger volumes, the cost per watt will probably still be higher, due to the higher cost of, for example, casing and connectors. However, since the cost of the inverter adds little to the overall cost of a PV-module, it can still be more cost-efficient to use decentralised inverters as a higher energy yield can be obtained in locations where shadows are present.

As small-scale inverters tend to have lower efficiency than larger inverters, it is important to optimise the control circuits and to choose a topology with the lowest possible power dissipation, if they are to compete with conventional inverters. The purpose of this paper is to compare eight different configurations with decentralised inverters and one conventional configuration. This comparison will

suggest an optimal configuration with respect to efficiency and cost. Both DC-buses and low voltage AC-buses, as well as grid-buses have been studied.

2 Pre-requisites and Method

From earlier studies of the Sankt Jörgen PV-plant, which is an experimental plant of 7 kW_p (peak power), it was concluded that shading was a major problem of energy production losses. To examine the possible power increase of this installation, decentralised inverters with a module oriented system were selected. This means that the power converters were designed for the PV-modules used: GPV110M, peak-power 110 W at 34 V (25-50 V). The energy produced is to be fed into the utility grid of the European standard: 230 V 50 Hz (single phase), which implies that a DC-link-voltage of 350 V is needed.

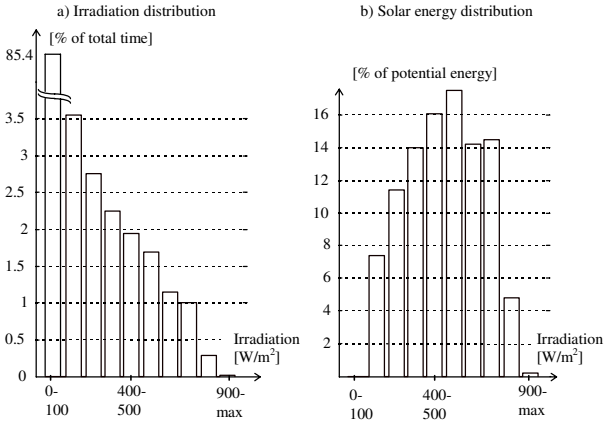

Fig. 1: Distribution of projected solar irradiation in southern Sweden 1994.

Since the aim, here, is to utilise the expensive PV-modules better, the most important consideration is, of course, efficiency. Considering statistics from sun irradiation in southern Sweden, Fig 1a, it is important that weighted energy efficiency is used since the inverter will operate substantially at lower load. Fig. 1b shows potential energy distribution (Fig. 1a multiplied by the power) from which it can be concluded that most energy is captured in the mid-power range.

Other considerations are cost, production ability, and safety. The first two are difficult to determine without an extensive investigation. Therefore, the figures presented here are just rough estimates.

3 Models for Estimating Power Loss

To calculate efficiency, relatively simple models of the components have been used. The values presented are not intended to be actual values but relative values for the purpose of this comparison. Only the main circuits (Figs. 5 to 13) have been considered. As mentioned, the power consumption of the control circuit of the inverter will affect overall efficiency, especially for these small-scale inverters and especially in PV-applications where they work more often at low load. *However*, the controllers have been assumed to consume approximately the same power and, therefore, will not affect this comparison.

3.1 Diode loss model

Diodes are used as non-controllable switches at relatively high frequency. Diodes with low conducting losses and soft recovery should, therefore, be chosen, for example schottky diodes.

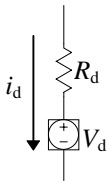

Fig. 2: Loss model for diodes.

For diodes, a constant forward voltage drop, $V_{d,}$ in series with a resistance, $R_{d,}$ is used to approximate the conducting losses at different currents, Eq. (1). $I_{diode,AV}$ is the average value of the current through the diode, i_d, and $I_{diode,RMS}$ is the root mean square value. Two different values of V_d have been used depending on the specific demand on reverse voltage and current in each circuit.

$$P_{diodes,Cond} = V_d I_{diode,AV} + R_d I^2_{diode,RMS} \qquad (1)$$

3.2 Transistor Loss Model

For low power and low voltage applications, the natural choice of transistors is MOSFET. The transistors are controlled as switches. In the off state they do not conduct and in the on state, the MOSFETs act as a resistor. Two different "on" resistance, r_{DSon}, have been used depending on the voltage level they are intended to withstand in each circuit. The conducting losses have been calculated as:

$$P_{transistors,Cond} = r_{DSon} I^2_{transistor,RMS} \qquad (2)$$

Switch losses for the MOSFETs have been estimated according to the following assumption. When the gate is driven by a current source, $I_{g,}$, the commutation of the current I_L from the diode, D, to the transistor, T, will ideally appear as inFig. 3. V_T is the threshold voltage of the MOSFET and V_Z is the threshold voltage of the zener diode. The energy dissipated during turn-on is approximately:

$$E_{ON} = \frac{I_L U_d}{2} t_1 + \frac{I_L U_d}{2} t_2 = \frac{I_L U_d}{2} \cdot (t_1 + t_2) \approx \frac{I_L U_d}{2} t_{sw} \qquad (3)$$

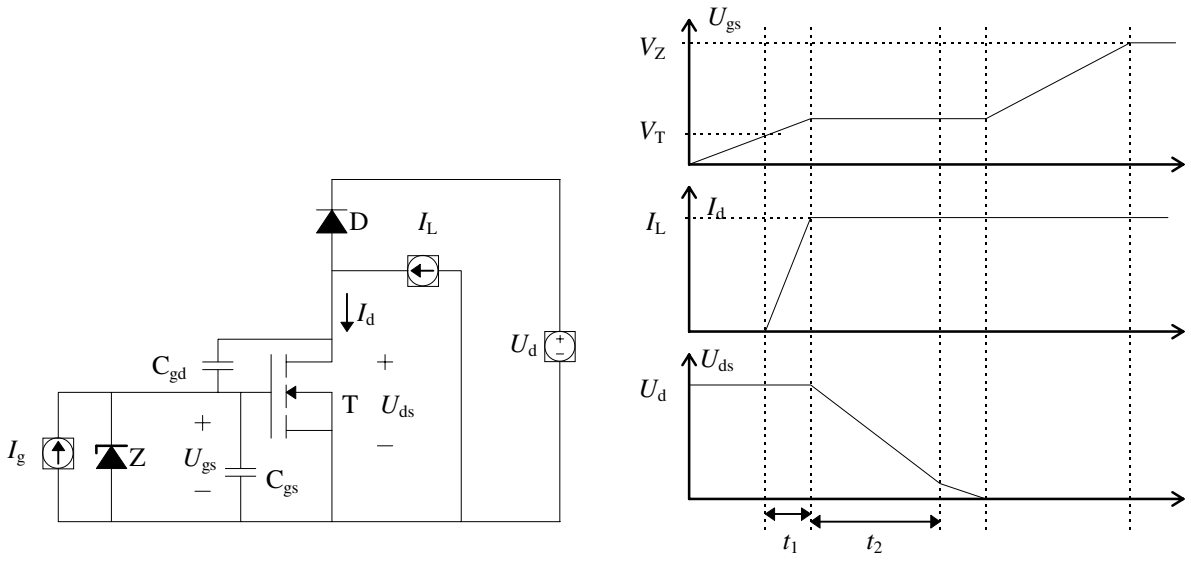

Fig. 3: Model for MOSFET switch losses

Turn-on and turn-off have been treated equally and have been repeated at the switching frequency f_{sw} which gives switching losses of:

$$P_{transistor,sw} = f_{sw} t_{sw} I_L U_d \qquad (4)$$

where $t_{sw} = t_1+t_2$. Note that the current through the diode first decreases to zero before the voltage reverse raises which gives zero switch losses for diodes commutating in parallel with the MOSFETs. (In reality reverse recovery current of the diode will make this loss non zero).

3.3 Transformer and inductance loss model

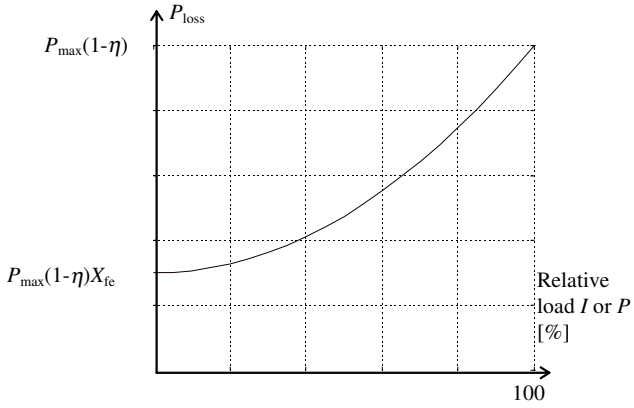

Fig. 4: Losses in iron/copper-components are modelled by a constant fraction and a load dependent.

Losses in transformers and inductances in switched applications are difficult to determine analytically. Normally, empirical formulas or tables from the manufacturer of the specific core material are employed. In addition, the losses are difficult to measure.

For the study, the assumption that the losses can be divided into one constant part and one that depends on the square of the load, Fig. 4, has been used. The constant part is due to the switching; hysteresis and eddy current losses in the core and ripple current losses in the copper windings. The non constant part is mainly resistive losses in the copper windings.

It is supposed that the efficiency, η, of the inductor or transformer at full load, is known. The fraction constant losses, X_{fe}, depends on the core material, the width of the range of the B-H-curve, the frequency used, etc. Filter inductances which operate at a relatively constant flux density have a negligible fraction of iron losses. A 50 Hz transformer on the other hand, which uses the B-H-curve's full range normally has iron losses of the same order as copper losses at full load. In Table I, the five different values of the iron/copper model are listed. The following Equation has been used:

$$P_{loss} = P_{max}(1-\eta)\left(X_{fe} + (1-X_{fe})\left(\frac{I}{I_{max}}\right)^2 \right) = [const.U] = P_{max}(1-\eta)\left(X_{fe} + (1-X_{fe})\left(\frac{P}{P_{max}}\right)^2 \right) \quad (5)$$

Type 1 is a filtering inductor at high frequency (HF) (tens up to a hundred kHz) with a ferrite core. The ripple in flux density is very small compared with B_{max} and so the value X_{fe} is mainly resistive losses from the current ripple.

Type 2 is an HF-transformer working in quadrant 1 of the B-H-curve (fly-back and forward converters).

Type 3 is an HF transformer working in quadrants 1 and 3 (square wave transformer).

Type 4 is a small (110 VA) line filter at 50 Hz and with an additional ripple at a few kHz. Core of iron powder.

Type 5 is a large (900 VA) transformer or line filter at 50 Hz (with an additional ripple).

Table I Different values for transformers and inductances

	Type 1	*Type 2*	*Type 3*	*Type 4*	*Type 5*
Total maximum losses (1-η)	1%	2%	3%	3%	2%
Fraction constant losses X_{fe}	5%	30%	60%	50%	50%

For PV-application where the inverter will most often work at a lower power rate, efforts must be made to keep the constant fraction, X_{fe}, low.

3.4 Capacitors

Capacitors are assumed to be ideal since their contribution to the total losses are very small. However, in the actual design, it is important to be aware that electrolytic capacitors often set limits on the inverter lifetime, mean time between failure (MTBF) and operating temperature.

4 The Nine Inverter/Converter Topologies

Innumerable topologies can be imagined to fulfil the demand; to convert the low voltage electric energy from the photovoltaics to an appropriate level for the grid. This chapter briefly presents the nine topologies selected.

4.1 Centralised inverter (or string inverter): C

The conventional connection for a PV-system is shown in Fig. 5, with PV-modules connected in series to create a sufficiently large voltage. A centralised full bridge-inverter transports the energy from the PV-generator to the grid. The inverter topology is a straight forward solution using as few components as possible. Optionally, a transformer could be used to insulate the voltage of the PV-plant from the grid. An advantage of this is that vagabonding currents are prevented. If the PV-modules are mounted on a grounded, conducting plate they will form a relatively large capacitor to the ground and due to the PWM-switching a leakage current will be drained through this capacitor. The disadvantages of this conventional topology are shading problems and non fault tolerance. When using only one inverter, which occasionally trips, there is no energy production until it is replaced or repaired.

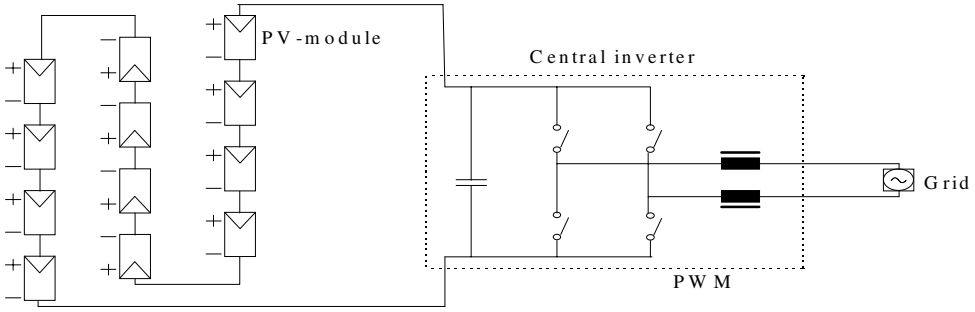

Fig. 5: Several PV-modules in series to one inverter.

4.2 A boost converter with a central inverter: DC1

A boost converter loads the PV-module optimally and boosts the input voltage from 25 - 35 V up to the bus level of 100 V, Fig. 6Fig. 6. The desirable 350 V cannot be reached in this step since it is difficult to boost up the voltage more than 4-5 times, due to resistance in the inductance L1. In the central unit, the current is inverted to AC and transformed up to an appropriate grid level. An advantage of this system is that batteries can easily be connected to the bus to obtain a stand alone system. The input current, I_{dc1a} is relatively smooth, therefore, the input capacitor, C1, may be small or omitted.

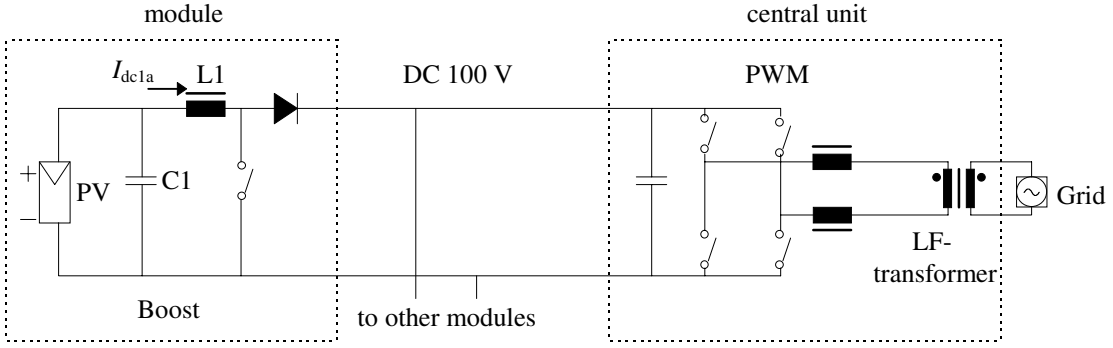

Fig. 6: A boost converter at every PV-module feeds a central inverter.

4.3 A forward converter feeding the bus: DC2

A forward converter is capable of boosting the input voltage up to the desirable 350 V. This gives a very simple topology for the central unit, shown in Fig. 7. The drawbacks are: The input capacitor, C1, must be quite large due to a large input current-ripple; the bus will hold square-wave jumping potentials which leads to high emissions of EMI and possibly stray currents. A relatively high DC voltage on the bus also reduces the safety of the personnel.

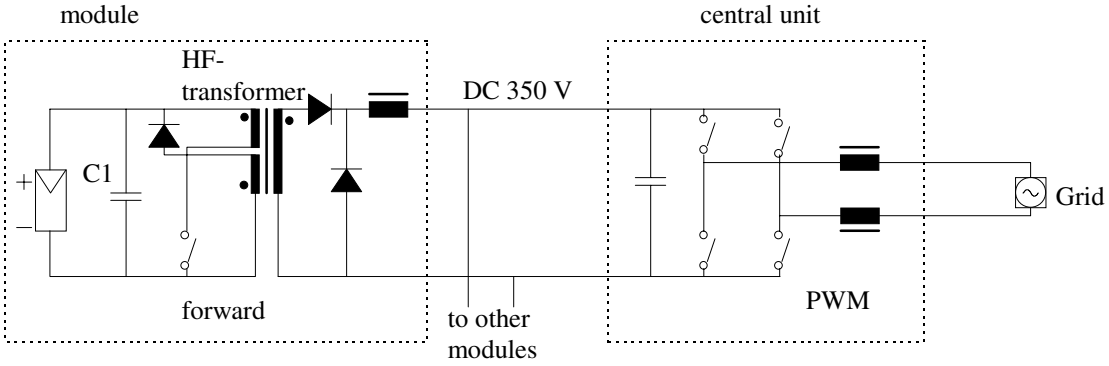

Fig. 7: A forward converter at every PV-module feeds a central inverter

4.4 A low Voltage AC bus: LVAC1

With a PWM controlled H-bridge connected directly to the PV-module, the energy is transformed to 50 Hz AC and centrally transformed up to grid level, as shown in Fig. 8. This results in a bus that is easy to handle and which has a non dangerous voltage level. However, the distance to the central transformer must be kept short due to relatively high currents and, therefore, high resistive losses in wires. The trade-off, when deciding the bus voltage is on one hand, that it's peak value must be lower (with a margin) than the voltage from the PV-module, even at low irradiation. On the other hand, a lower bus voltage results in lower efficiency.

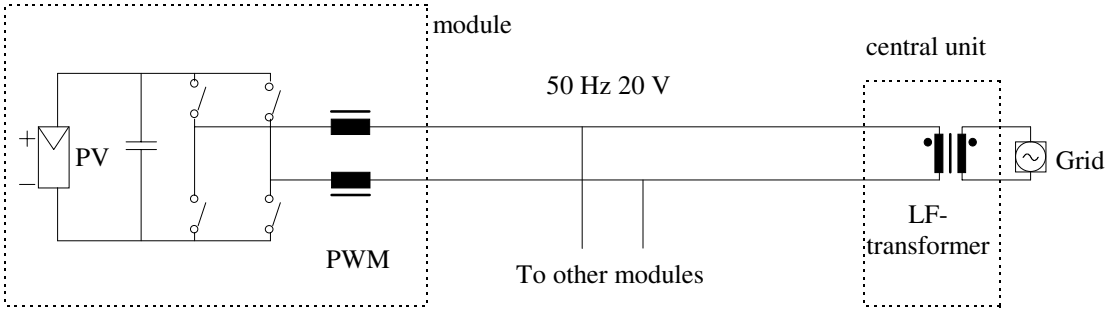

Fig. 8: An inverter at every PV-module feeds a low voltage AC-bus.

4.5 Two Zeta converters in anti-parallel: LVAC2

This topology has been proposed by Myrzik et. al [3] but with a higher input voltage so the central transformer is superfluous, which is why the comparison here is somewhat unfair. The two Zeta converters, shown in Fig. 9, supply each half period of the 50 Hz current. During the first half period, switch 4 is on and switch 1 is controlled with a PWM pattern to form the current sinusoidal. For the subsequent half period, switch 3 is on and switch 2 forms the current. With this arrangement, two switches are saved compared with a single converter forming the current and a full bridge switching each half period to the grid at each polarity. Critical components in this topology are C2 and C3 which must transfer the total power (in contrast to filter capacitors).

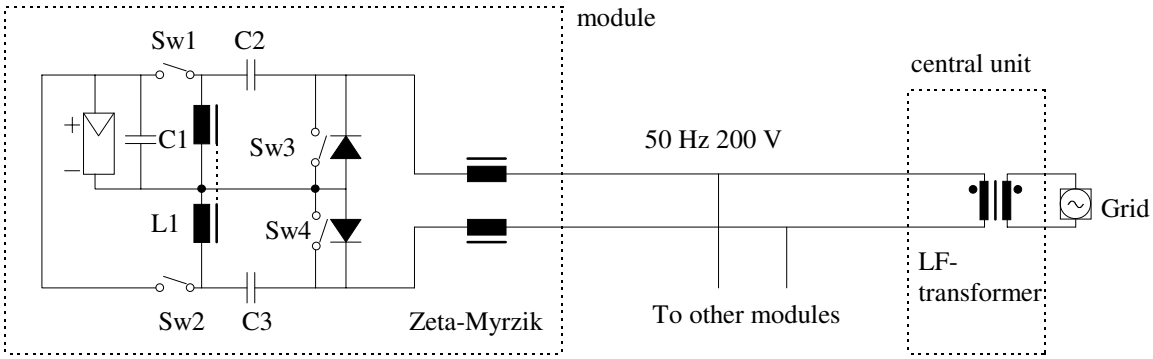

Fig. 9: Two zeta converters forming each half period of the current out.

4.6 A Fly-back converter feeding a PWM inverter: AC1

In Fig. 10, a fly-back converter boosts up the input voltage to the desirable level on the DC-link, V_{ac1}. The main feature of the fly-back is the transformer, Tr, which acts both as the main inductor and transformer so only one iron/copper-part is needed for the voltage boosting. This stage is controlled to obtain maximum energy from the PV-module and the H-bridge keeps the dc-link, V_{ac1}, at a constant voltage and transports the energy to the grid.

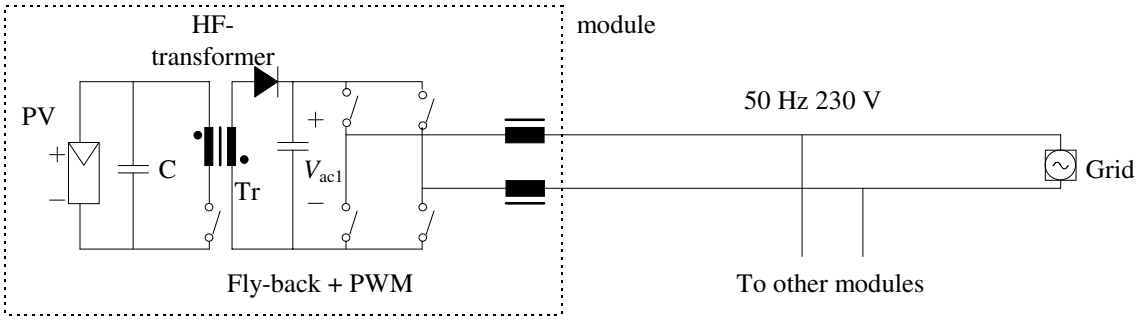

Fig. 10: A fly-back converter feeds a inverter wich is connected to grid.

4.7 A Forward converter feeding a PWM inverter: AC2

This topology (AC2) is very similar to the previous one (AC1), but the voltage step-up is now performed by a forward converter.

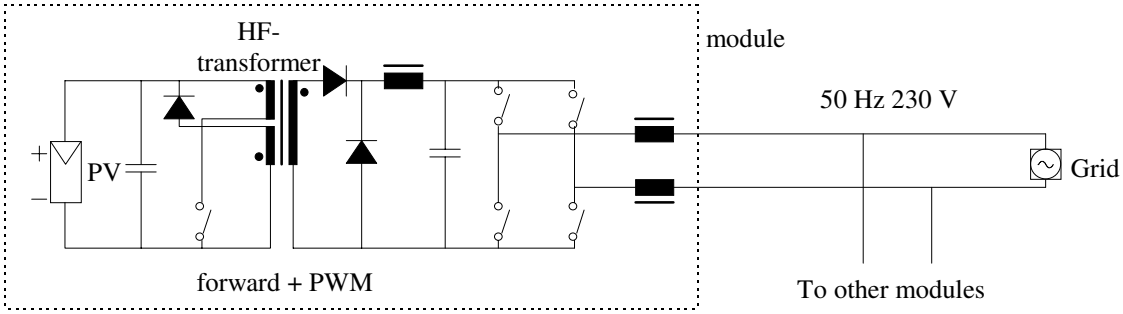

Fig. 11: A forward converter feeds a inverter wich is connected to grid

4.8 A three stage inverter: AC3

The topology in Fig. 12 has been designed to handle very large voltage step-ups [4], from 2 V, 100 A on the input to 350 V in the second DC-link, V_{ac3b}. A soft switching mode for the first stage is achieved by adding a switch-over inductor L1 and D5. The two first switches are alternately "on" at a

duty cycle of 50% which takes the input voltage to a hundred volt after the rectifier bridge, V_{ac3a}. In the next stage, a boost converter is controlled to load the PV module optimally and it boosts up the voltage to the desirable 350 V. The input current, $I_{ac3a,}$ is relatively smooth except for transitions between switches 1 and 2, thus the input capacitor, C1, may be kept small.

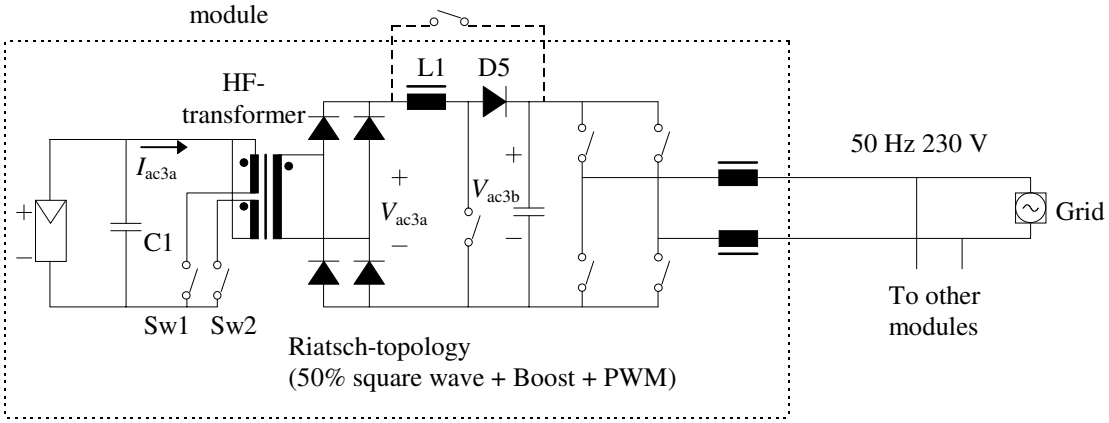

Fig. 12: Three stages; square wave transformation, boost converter and a PWM-inverter.

4.9 A Square Wave Transformer feeding a PWM inverter: AC4

The primary H-bridge feeds a square wave current to the transformer which is employed to boost up the voltage to 350 V at the DC-link, V_{ac4} in Fig. 13. L1 takes care of voltage differences during switch transitions but might be omitted if the transformer's transfer inductance is high enough. The second H-bridge will both form the output current and find the optimal load of the PV-module.

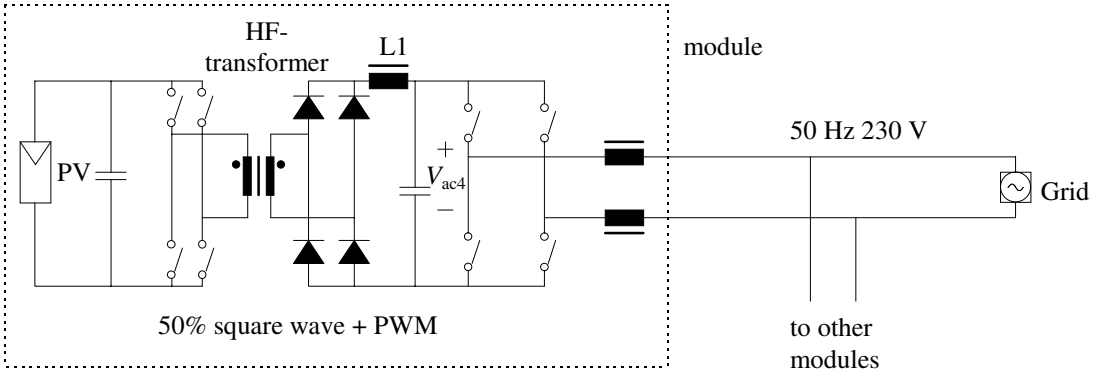

Fig. 13: A quare wave transformer boosts voltage to PWM-inverter.

5 Calculations and Results

The following parameters have been used for calculations: 12 PV-modules in one system. For low-volt-diodes V_d=0.37 V, high-volt-diodes V_d=0.5 V and dynamic diode resistance, R_d=67 mΩ. For low voltage MOSFETs r_{DSon} is set to 22 mΩ while r_{DSon}=350 mΩ for high voltage MOSFETs. A 100 kHz switching frequency is used for converters, 5 kHz for inverters and the switching time t_{sw} of 150 ns.

Energy efficiencies have been calculated (Table II, 1st row) from the described models with the parameters listed above. The sensitivity in parameter change has been investigated by changing the parameters one by one within reasonable values. By doing this, the resulting energy efficiency was somewhat changed but still three groups could be identified: 95 % efficiency for C, 85-90 % for DC2, LVAC1, LVAC2 and AC1 and finally DC1, AC2, AC3 and AC4 which had an energy efficiency lower than 85 %.

Table II Values from energy efficiency- and cost-calculations

Topology	C	DC1	DC2	LVAC1	LVAC2	AC1	AC2	AC3	AC4
Energy efficiency	94,9%	82,4%	86,6%	88,0%	87,4%	86,1%	80,4%	77,5%	79,0%
Cost [Euro] /module	15,28	62,72	77,91	59,56	95,06	104,25	113,00	111,50	110,25
Continues current in	No	Yes	No	No	No	No	No	Yes	Yes
Local insulation	No	No	Yes	No	No	Yes	Yes	Yes	Yes
Central insulation	No	Yes	No	Yes	Yes	No	No	No	No
Fault tolerant	No	No	No	Yes	Yes	Yes	Yes	Yes	Yes

The cost is estimated for each topology by the prices of the components (in 100s) in the main circuit and control circuit. For systems with central devices (all but AC1 to AC4) the cost of the central parts are divided by the number of PV-modules (12). Note that even if the cost per module is 4-7 times the C-topology, the cost should be put in relation to the PV-module price, which is 450-600 Euro. This means if the energy production loss due to shading for topology C is greater than 10-20 %, decentralised topologies are more cost efficient. Moreover, the small-scale inverters have a greater potential for cost reduction when produced in larger volumes (machine mounting, no heat sink, no wires etc.).

Topologies that load the PV-module with a smooth, continuous current, can have a smaller or no capacitor at all on the input (Table II, 3rd row) which implies higher reliability. Additionally, it is easier for the maximum power point controller to track the maximum power point without a significant ripple in current and voltage. Local insulation, in Table II, simply means that a transformer is employed in the decentralised unit while the central insulation is one central transformer.

Only topologies with no central unit (AC1 - AC4)are true fault tolerant. The modules work independently and if one device trips, the remaining modules will still operate (unless the bus has short circuited). However, in LVAC1 and LVAC2 the central unit consists of a single transformer (a few kVA), which can be considered to be a very reliable component. Therefore, even these topologies are considered to be fault tolerant.

6 Conclusions

The centralised inverter, C, has superior efficiency and also the lowest cost per watt, so if the intended PV-plant has minor problems with shadings, this is a good choice. A transformer can be added to obtain an insulated system, which eliminates stray currents, and improves the safety of personnel at the cost of lower efficiency.

Among the decentralised topologies, the LVAC1 is somewhat outstanding in high efficiency and low cost, but other considerations might be conclusive, for instance, the choice of bus. If DC loads are to be used, or if a stand-alone system with batteries is desirable, a DC1 might be preferable. In another case, if a true modular system is desirable where you can start with one PV-module and one small-scale inverter to extend the system later, then, an AC1 might be the choice.

Another concern of interest, which is not within the scope of this study, is harmonics on the grid. How do systems with hundreds of small-scale inverters affect the power quality on the national grid? Which harmonics are added together and which cancel? Topologies C, DC1 and DC2 avoid these questions by having only one inverter with known or measurable harmonics.

The selection for the modification of the Sankt Jörgen PV-plant has been topology LVAC1 due to its relatively high energy efficiency and low cost. It has few components, which implies long MTBF and robustness. The central transformer can, to some extent, filter harmonics generated by the inverters, to the grid.

Some drawbacks are, as mentioned, the relatively high currents on the bus. In addition, the control circuit, sensors and power supply are somewhat more complex to realise compared with the DC1 and DC2 topology. The topology has a minimum input voltage level which together with the I-V-cure for the PV-module sets limits to energy production at low irradiation. The input capacitor must be quite large to reduce the 100 Hz ripple on the input current.

The LVAC1 system has been designed, built and functionally tested but further optimisations, measurements and evaluations are forthcoming.

7 References

1. Henk Oldenkamp, Irene de Jong. *Next Generation of AC-module Inverters*, 2nd World Conference and Exhibition on Photovoltaic Solar Energy Conversion, Vienna 1998.
2. W. Kleinkauf. *Photovoltaic Power Conditioning / Inverter Technology*, 10th EPVSEC, Lisbon 1991.
3. Johanna Myrzik. *Power Conditioning of Low Voltage Generators with Transformerless Gridconnected Inverter Topologies*, 7th European Conference on Power Electronics and Applications, Trondheim 1997.
4. J.Riatsch, H. Stemmler, R. Schmidt. *Single Cell Module Integrated Converter System for Photovoltaic Energy Generation*, 7th European Conference on Power Electronics and Applications, Trondheim 1997

A 110 W Inverter for Photovoltaic Applications

B. Lindgren
Department of Electric Power Engineering
Chalmers University of Technology
SE-412 96 Göteborg
Sweden

Abstract: Photovoltaics have the potential to supply society with energy with very little environmental impact. If the energy is to be distributed to the national grid, the dc-quantities of the PV-cell have to be converted to ac-quantities adapted to the existing grid. This paper presents the design of and measurements from a module-oriented inverter of 110 W. The current controller is implemented in an inexpensive 8-bit micro controller, which uses a hysteresis technique also known as bang-bang control. Emphasis has been put on high energy-efficiency (over 90 %) and high power quality (THD_i 8.8 % all frequencies).

Keywords: Inverters, Photovoltaic power systems, Solar power generation, Fault tolerance, Bang-bang control, Current control, MOSFET circuits.

I. INTRODUCTION

Photovoltaics (PV) or solar cells have the potential to supply society with energy with very little impact on the environment [1]. The cost of the PV has been reduced during the past decades but is still too high to compete with conventional energy sources. Nevertheless, for remote applications PV can be the best choice from an economic point of view. However, since governments all around the world have realised the necessity of changing to more sustainable practices, large programmes have been initiated to stimulate the growth of PV in, e.g. the USA, Japan and Europe.

To make use of the expensive PV, it is important not only to position the PV-modules in an optimal way *but also* to consider the electrical behaviour of the cells [2]. Production losses due to shading effects are extensive in many PV-plants: For example, in the German 1000-roofs-PV programme, 10-15 % of the losses were due to shading [3]. Every measure should be taken to minimise shading, although sometimes it cannot be avoided. In such cases, a more shade-tolerant system should be employed. The fewer PV-cells connected to one converter the higher the shade-tolerance obtained. The disadvantage of such a system is its higher auxiliary power consumption and therefore lower power efficiency. However, the energy yield of a decentralised configuration can still be higher than that from a conventional system if shading is present. Additionally, the system becomes more modular, which makes it easy to exchange modules or expand an existing system with new modules.

An evaluation of the PV-plant at St Jörgen, Göteborg, Sweden has shown that energy loss up to 30 % could be derived from shading effects even though only a very small fraction of the PV-cells was shaded [4]. This paper presents a module-oriented inverter that decreases this loss drastically.

II. SELECTION OF SYSTEM CONFIGURATION

An investigation has been performed to compare different decentralised configurations and one conventional configuration [5]. Fig. 1 shows a conventional system configuration and a decentralised system.

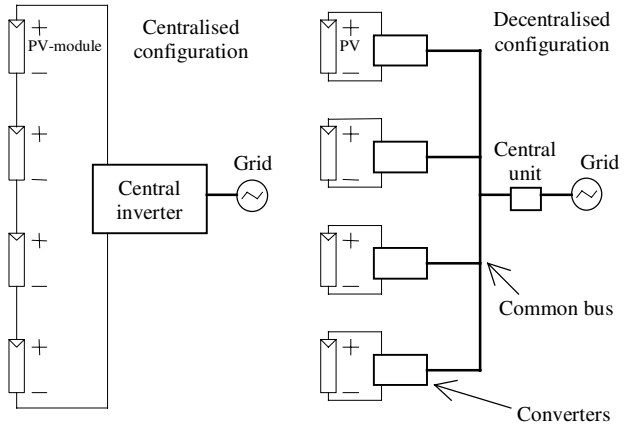

Fig. 1 A centralised configuration and a decentralised.

In case of a centralised configuration, one converter takes care of the power from a large number of PV cells, while for a decentralised configuration, the PVs are arranged in smaller modules independent of each other and each connected to a common bus. The common bus could be of different types: DC, low voltage AC or the grid. The result has shown, not surprisingly, that one central inverter gives the highest energy efficiency and lowest cost, *provided* no shading effects are taken into account. Among the decentralised configurations, a low voltage AC bus proved to be the most favourable solution.

In the selected configuration, Fig. 2, each PV-module is connected to a transistor inverter. Each inverter operates its PV-module at the maximum power point and feeds a sinusoidal current into a low voltage AC-bus. A one-phase- or a three-phase-transformer boosts the voltage up to the grid level of 230/400 V. The transformer can be considered to be very reliable, so the system becomes fault-tolerant as the modules work independently of each other and if one fails, the others will keep on operating.

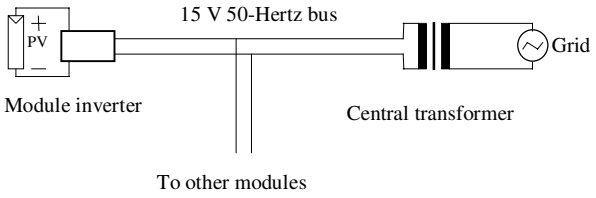

Fig. 2 The selected configuration with a low voltage AC-bus.

III. DESIGN OF THE INVERTER

The aim is to design a cheap inverter that can be mounted onto the back of a PV-module, that is easy to connect to the common bus. The voltage from the PV-modules used (GPV110M) is 25-50 V and a maximum power of 110 W. The factors to be considered during the design phase are the selection of switches, capacitor and inductors, however, the control of the switches is also an important issue.

A. Main Circuit

The main circuit can be seen in Fig. 3. The H-bridge consists of four MOSFET-transistors. A capacitor, C, makes the voltage source stiff and two inductors, L, filter the output current to the low voltage AC-bus.

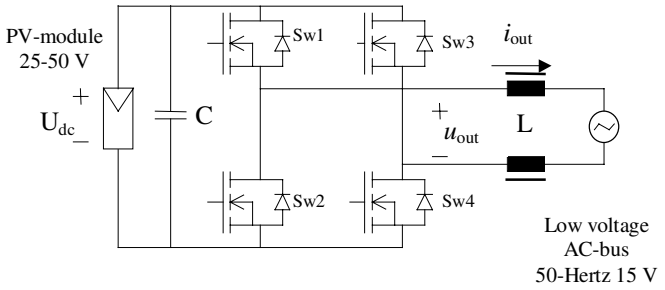

Fig. 3 Main circuit.

An H-bridge can apply $+U_{dc}$ (Sw1 and Sw4 on), $-U_{dc}$ (Sw2 and Sw3 on) or zero voltage (Sw1 and Sw3 on *or* Sw2 and Sw4 on) at the output, u_{out}. To force current into the AC-bus, the dc voltage, U_{dc}, must be higher than the top value of the bus voltage in order to create a sinusoidal current.

The choice of switches is naturally the MOSFETs for low power and low voltage applications. The MOSFETs have very low conducting losses (R_{DSon} of 8 mΩ available for 55 V, 100 A transistors) and are also easy to control quickly which gives low switching losses. Additionally, they have parasitic, anti-parallel diodes that can be used as freewheel-diodes. If these diodes show a poor performance (long reverse recovery time or high forward conducting voltage) external diodes, preferably schottky diodes, should be used in parallel. The selected MOSFETs: HRF3205, have been tested with and without schottky diodes of the type: IR50SQ100. The difference was not measurable so the diodes have been omitted.

The capacitance on the DC-link supplies the H-bridge with a stiff voltage. Dimensioning is such that the 100 Hz ripple on the voltage is kept within reasonable values. A capacitance of 2200 µF gives a worst-case ripple of 3 %. The capacitor must also be able to carry a fairly high current; roughly 1.5-2 times the mean dc current. A capacitor with a low equivalent series resistance should be employed, due to the filtering function and to minimise the heat-up of the capacitor in order to avoid shortening its lifetime.

The design of the inductors, L, is important, considering both power quality and efficiency. The core material together with the variation in flux density determines the iron losses (eddy currents and hysteresis). If the switching frequency is increased, the ripple losses will normally decrease (not for the fundamental frequency though), but then the switching losses in the transistors will increase. A high inductance will also reduce the ripple current and, therefore, decrease the ripple losses but, on the other hand, will increase the conducting (copper) losses and, of course, increase the weight and cost of the inductance. The inductance was selected with empirical data (see section 'Results and Measurements').

B. Control Circuit

The block diagram of the main circuit and of the controller is shown in Fig. 4.

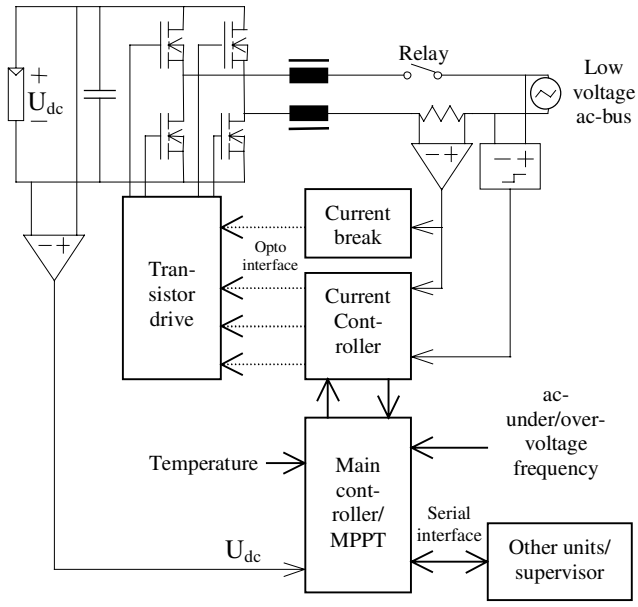

Fig. 4 Block diagram of the inverter.

The main controller, referred to as the maximum power point tracker (MPPT), has the overall responsibility. Initially, it checks the AC voltage, the frequency and the DC voltage. The

MPPT gives start and stop commands, and the reference value of the current (power) to the current controller. In return, it receives three values per 50-Hertz cycle from the current controller: the energy produced, the error sum and the number of samples. From these values and from the DC-voltage, U_{dc}, the MPPT determines whether or not the reference value should be increased or decreased to find the maximum power point. It continuously checks the AC-bus frequency and voltage for grid failure. It is also capable of measuring the temperatures of the transistors and, optionally, of the PV-module. The MPPT is able to collect data, such as produced energy and different error states and store them in a non-volatile memory and later report to a supervisor via a serial interface.

For convenience, a special transistor drive circuit has been used: IR2113. The blanking time for the switching schemes is realised by an RDC-link at each input of the IR2113, with a switch-on delay of approximately 1 µs. To minimise energy consumption, logic latches are implemented to 'freeze' the output voltage-state and the power-consuming opto-couplers are only activated for 200 ns at each change.

The current controller controls the H-bridge switching. This is a micro controller that uses a hysteresis technique. It synchronises a timer to the zero crossings in the grid voltage. From this point, a look-up-table is used to produce a sinusoidal curve shape. This is then multiplied by the mean current value coming from the MPPT-controller. The product is the reference current. Around this reference, the current controller sets an upper and a lower limit for the current, of approximately +/-0.3 A, as shown in Fig. 5.

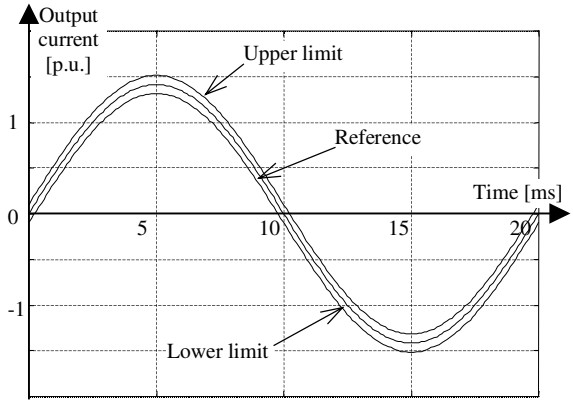

Fig. 5 Limits for shaping the output current

If the current is lower than the lower limit, the current controller switches the H-bridge to increase the current and vice versa. Due to the varying bus voltage, the derivative of the current will vary during the 50-Hertz cycle. Hence, different outputs are applied depending on what region of the 50-Hertz cycle is being controlled. When switching close to the grid top voltage, $+U_{dc}$ puts only a few volts across the inductance, while $-U_{dc}$ would give a negative inductor voltage of the order of several tens of that value. Therefore, switching between $+U_{dc}$ and 0 gives a less asymmetrical control performance. Close to zero voltage in the grid, U_{out} is forced onto L and to obtain a symmetrical control performance, $+U_{dc}$ and $-U_{dc}$ have been used here. In Fig. 6, i_{out} is shown on top and u_{out} is shown below with the different regions of applied voltage levels.

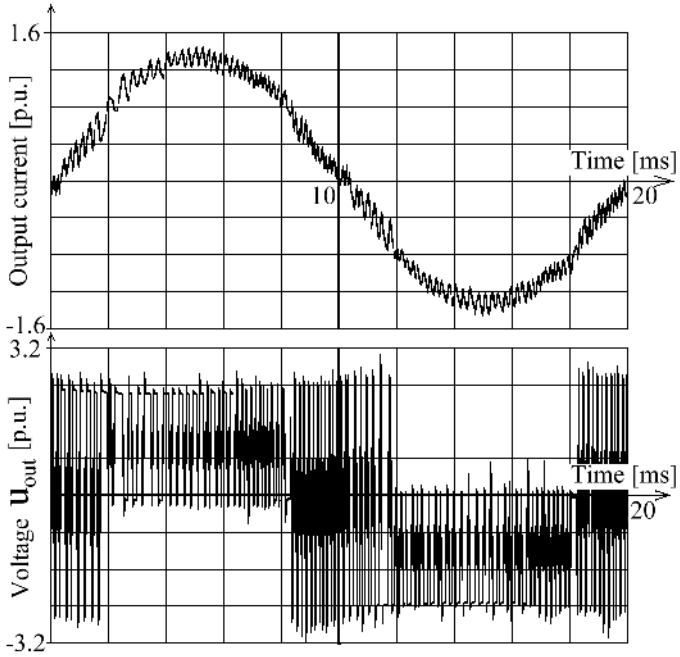

Fig. 6 Output current and output voltage.

Although the micro controller is fast (AT90S2313 at 10 MIPS) it has a loop time of approximately 34 µs. One programme loop starts by sampling the actual current (10-bit ADC) and calculating the reference value. Some cumulative variables are calculated and finally, the current controller determines whether or not to change the output voltage. This means that the current is sampled in the beginning of the loop while the control is done at the end of the loop. To improve performance, the current controller uses the previous and actual value of the current to predict the current value at the control instant. It is the predicted current rather than the actual value that has to be within the tolerance band. This is possible due to a good circuit design with a relatively low noise-level. For the example in Fig. 7, this means that the current controller would change the output voltage so that the current starts to decrease, even though the actual value has not exceeded the upper limit.

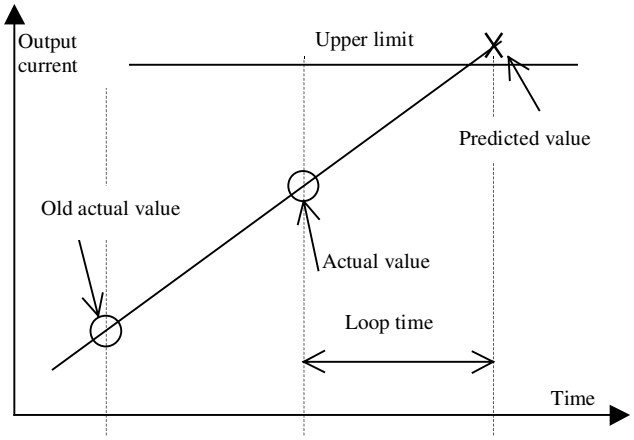

Fig. 7 The current controller controls on predicted current.

During the loop after a change in output voltage, the calculation of the predicted value is skipped due to an uncertainty in the current form at this moment. Instead, only the actual value is checked.

IV. RESULTS AND MEASUREMENTS

Fig. 8 shows the realised 110 W-inverter. At the bottom of the casing the main circuit is situated, with the four MOSFETs, the DC-link capacitor, the inductors and the drive circuits. On the lid, a circuit board with the controller, current sensor, over current protection and the two micro controllers are situated.

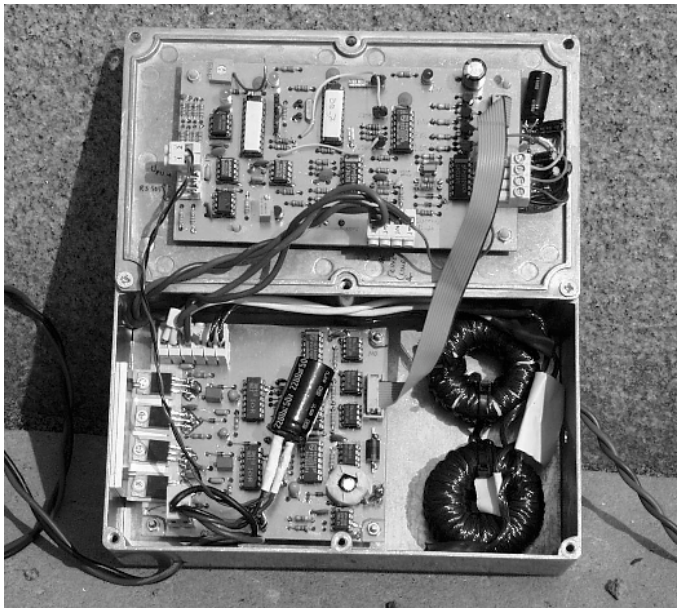

Fig. 8 The prototype of the 110W inverter.

A. Efficiency

To maximise the efficiency, different switching strategies and different designs of the inductors have been tested. One problem in measuring the efficiency is the temperature dependence of the components, which can have a rather large impact on the efficiency. To minimise these effects, all measurements have been performed in a similar procedure with intervals between the measurements to let the temperature stabilise.

The switching strategy has been improved in several steps and the one used is described earlier in the section 'control circuit'.

Several inductors have been tested, with similar results. The four compared here are presented in Table 1. Figures in parentheses are normalised in p.u. (P_n=110 W and U_n=15 V).

TABLE 1. Four of the tested inductances

	L1	L2	L3	L4
L_{HF} [mH (p.u.)]	1.8 (0.28)	1.4 (0.21)	1.0 (0.16)	1.7 (0.26)
L_{LF} [mH (p.u.)]	2.8 (0.42)	2.2 (0.34)	2.3 (0.35)	2.3 (0.35)
Quota L_{LF} /L_{HF}	1.5	1.6	2.2	2.3
Iron powder core	Two large	One with air gap	One	Two
Windings [turns]	110 & 110	57 + 51	33 + 38	81 & 60
THD_i	7.0 %	8.8 %	12.7 %	8.6 %

L1 is winded on two, large toroids (2.8 times the volume of the others) of iron powder. It has fairly high losses, probably due to having a different material than the others. L2, L3 and L4 iron powder toroid cores from Amidon (T-184-16). On L2 and L3, two windings have been made on the same core. L2 has an additional air gap, to reduce the magnetic flux. L4 is made of two toroid cores.

L_{HF}, in Table 1, has been determined by applying a step in the voltage, U_L, on the inductor and measuring the resulting current derivative. Equation (1) gives the inductance (at low current amplitude).

$$L_{HF} = \frac{U_L}{di_L/dt} \tag{1}$$

L_{LF} is the 50-Hertz inductance at nominal (sinusoidal) current, as defined below.

$$L_{LF} = \frac{U_{L,RMS}}{\omega \cdot I_{L,RMS}} = \frac{U_{L,RMS}}{2\pi 50 \cdot I_{L,RMS}} \tag{2}$$

Unfortunately, the characteristics of a B-H-curve for any magnetic material seem to make $L_{LF} \geq L_{HF}$. For smoothing the current, a high inductance, L_{HF}, is needed, while for the fundamental frequency, there is no need for inductance at all. The largest inductance that can be used at minimal dc-voltage is 1 p.u. Otherwise, the maximum derivative of the fundamental frequency cannot be reached. Therefore, it is desirable with a low quota L_{LF}/L_{HF}. As can be seen, L1 and L2 have lower values.

The most important feature of the inductance is low power dissipation as the inductor itself stands for 60-80 % of the total power loss for this inverter. In Fig. 9, the total loss of the inverter, including the auxiliary power supply, is plotted as a function of input power. L2 seems to have the lowest loss in the mid-range where a PV-inverter captures most of the energy and was selected to be used.

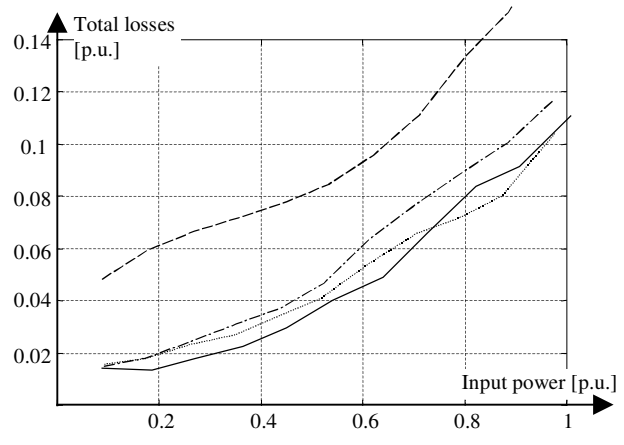

Fig. 9 Total inverter loss; dashed L1, solid L2, doted L3 and dot-dashed L4

The values in Fig. 9 have been calculated from (3). The average dc current, *ave(I_{dc})*, and the average of the ac power, *ave(P_g)*, have been calculated by the oscilloscope (LeCroy 9304CM), as indicated in (3). $i_{dc}(n)$ is the n:th sample of the dc current, $u_g(n)$ is the ac-voltage and $i_g(n)$ is the ac-current. The sampling rate used is 500 kS/s and approximately a hundred complete 50-Hertz cycles have been averaged in order to get the values.

$$P_{losses} = P_{dc} - P_g = U_{dc} \cdot ave(I_{dc}) - ave(P_g) = \tag{3}$$
$$= U_{dc} \cdot \sum_{100}(I_{dc}) \Big/ 100 - \sum_{100}(P_g) \Big/ 100 =$$
$$= U_{dc} \cdot \sum_{100} \left(\frac{\sum_{n=1}^{10000} i_{dc}(n)}{10000} \right) \Big/ 100 - \sum_{100} \left(\frac{\sum_{n=1}^{10000} u_g(n) \cdot i_g(n)}{10000} \right) \Big/ 100$$

The values in Fig. 9 converted to efficiencies give a top efficiency of 93.7 % at a 40 W input (0.35 p.u.). At full load, it decreases to 89.0 %. If the sun irradiation distribution in Lund, 1994 [5] is applied to the curve, and the irradiation less than 100 W/m^2 (10 %) is filtered, the total energy efficiency will be 92.7 %.

The calculations above are delicate since two almost equally large numbers are subtracted or divided, at least in the high power end. However, for the selection of the optimum inductance, only the relative measurement is important. As mentioned, the measurements were performed in the same manner and can, therefore, be considered to be relatively accurate.

B. Total Harmonic Distortion

Another issue of interest for inverters is the harmonics they generate. When tens or hundreds of inverters are connected to the grid it is very important to have output currents of good quality. If not, problems might occur on the grid, or in equipment connected to it.

To measure the distortion of the output current, the total harmonic distortion, THD_i, is often used. Equation (4) defines the THD_i used here (different definitions exist).

$$THD_i = \frac{\sqrt{\sum_{n=2}^{\infty} I_{(n)}^2}}{\sqrt{\sum_{n=1}^{\infty} I_{(n)}^2}} = \frac{\sqrt{I_{RMS}^2 - I_{(1)}^2}}{I_{RMS}} \tag{4}$$

In Table 1, the average THD_i values are presented for the four different inductances on the bottom row. An observation is that the higher the L_{HF}, the lower the THD_i. The choice of inductance is L2 mainly due to its low loss and fairly low THD_i.

The THD_i has been determined by measuring the output current at 5 MS/s. A complete 50-Hertz cycle has been captured and the I_{RMS} and the fundamental current, $I_{(1)}$, have been calculated by the oscilloscope. The THD_i was then calculated by (4) for ten captured 50-Hertz cycles and the average values and standard deviations of the THD_i were calculated. The standard deviation proved to be less then 0.2 for all four THD_i values.

A typical 50-Hertz cycle of the output current is captured in Fig. 10. The current is 5.9 A, thus, corresponding to the rated power of 110 W.

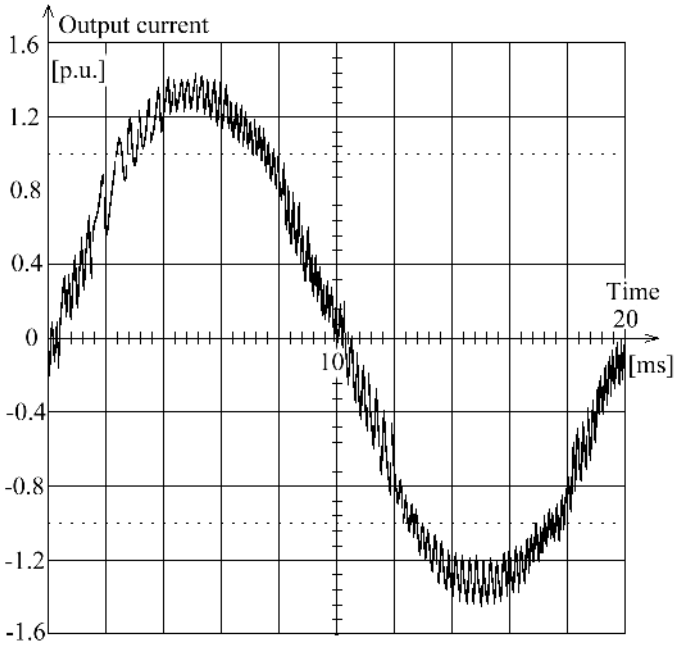

Fig. 10 A 50-Herz cycle of the output current.

A Fourier analysis shows that apart from the 5th and the 7th harmonics no particular frequency dominates, but the main harmonics are found up to 8 kHz, see Fig 11.

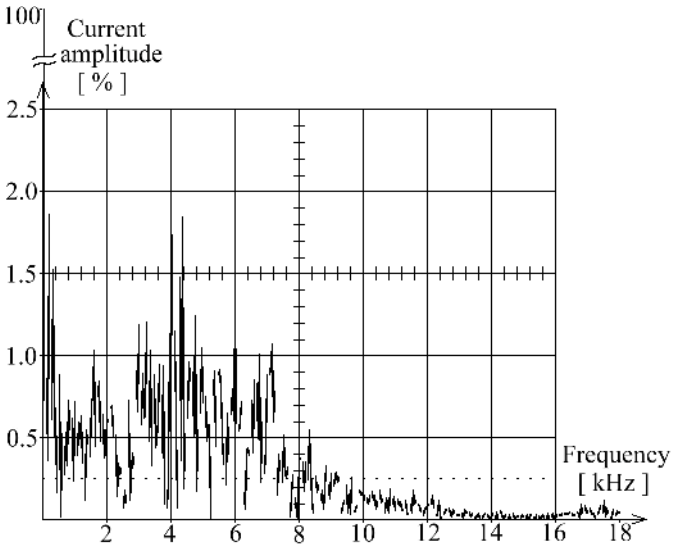

Fig. 11 A FFT of the current in Fig. 10.

Table 2 lists the six largest harmonics for this particular sample. No harmonics are larger than 2 % of the fundamental frequency and the frequencies above $I_{(7)}$ change from cycle to cycle since the hysteresis control is used.

TABLE 2. The largest harmonics of the current in Fig. 10.

I_{RMS}	I_{DC}	$I_{(1)}$	$I_{(5)}$	$I_{(7)}$	$I_{(61)}$	$I_{(66)}$	$I_{(82)}$	$I_{(88)}$
5.930	0.013	5.907	0.106	0.087	0.068	0.068	0.098	0.105
	0.22%	100%	1.8%	1.5%	1.1%	1.2%	1.7%	1.8%

The 5th and the 7th harmonic originate from the auxiliary power supply on the ac-side, which simply consists of a diode, a capacitor and a voltage controller. In Fig. 10, the consequence of this can be seen as an asymmetry in the *first half* of the positive and negative loop.

V. CONCLUSIONS

A one-phase inverter has been designed to be mounted on the backside of a PV-module. The input voltage is 25-50 V and the maximum power is 110 W. It delivers a sinusoidal current to a low voltage AC-bus of 15 V. The power is then transformed to grid level. Relatively cheap components and solutions have been selected to make an economically competitive design.

Efforts have been made to obtain a high efficiency, especially in the mid-range where the majority of the energy is captured. A top inverter efficiency of 93 % was reached at half load and 89 % at full load. This is somewhat better than the average inverter on the market [6].

When hundreds of inverters are connected together to the grid, it is important to keep the harmonics low. The THD for this inverter is less than 9 % and none of the harmonics generated exceeds 2 % of the rated 50-Hertz current.

VI. ACKNOWLEDGEMENTS

The Research Foundation at Göteborg Energi AB is gratefully acknowledged for its financial support.

VII. REFERENCES

[1] J. Rannels, “Trends in PV Technology Development – Future Implications”, Proceedings of the 2nd World Conference on Photovoltaic Solar Energy Conversion, ISSN 1018-5593, 1998, pp. LXXXVII-XCII.

[2] V. Quaschning, R. Hanitsch, “Increased Energy Yield of 50 % at Flat Roof and Field Installations with Optimized Module Structures”, Proceedings of the 2nd World Conference on Photovoltaic Solar Energy Conversion, ISSN 1018-5593, 1998, pp. 1993-1996.

[3] K. Kiefer et al “The German 1000-roofs-PV Programme — A Résumé of the 5 Years Pioneer Project for Small Grid-connected PV Systems”, Proceedings of the 2nd World Conference on Photovoltaic Solar Energy Conversion, ISSN 1018-5593, 1998, pp. 2666-1270.

[4] P. Carlsson, L. Cider, B. Lindgren, “Yield losses due to Shading in a Building-integrated PV Installation; Evaluation, Simulation and Suggestions for Improvements”, Proceedings of the 2nd World Conference on Photovoltaic Solar Energy Conversion, ISSN 1018-5593, 1998, pp. 2666-1270.

[5] B. Lindgren, ”Topology for Decentralised Solar Energy Inverters with a Low Voltage AC-Bus”, Proceedings of the 8th European Conference on Power Electronics and Applications, Lausanne 1999.

[6] H. Wilk, C. Panhuber, “Power Conditioners for Grid Interactive PV Systems, What is the Optimal Size: 50 W or 500 kW?”, Proceedings of the 13th European Photovoltaic Solar Energy Conference, 1995, pp. 1867-1870.

BIOGRAPHY

Björn Lindgren received a MSc degree in Engineering Physics from Chalmers University of Technology, Göteborg, Sweden in 1993. He has been working in the industry for four years, designing power electronics and control circuits. In 1997 he joined the Department of Electric Power Engineering at Chalmers as a PhD-student.